Title: A unified functional network target for deep brain stimulation in obsessive-compulsive disorder

Short title: Functional network target for DBS in OCD

Authors: Ningfei Li[1*,+], Barbara Hollunder[1,2,3+], Juan Carlos Baldermann[4], Astrid Kibleur[5,6], Svenja Treu[7], Harith Akram[8,9], Bassam Al-Fatly[1], Bryan Strange[7], Juan A. Barcia[10], Ludvic Zrinzo[8,9], Eileen Joyce[8,9], Stephan Chabardes[5], Veerle Visser-Vandewalle[11], Mircea Polosan[5,12,13], Jens Kuhn[4,14], Andrea A. Kühn[1,3], Andreas Horn[1]

** Corresponding Author*
[+] Both Authors contributed equally

Affiliations

1. Charité – Universitätsmedizin Berlin, corporate member of Freie Universität Berlin, Humboldt-Universität zu Berlin, and Berlin Institute of Health, Movement Disorders and Neuromodulation Unit, Department of Neurology, Charitéplatz 1, 10117 Berlin, Germany.
2. Charité – Universitätsmedizin Berlin, Einstein Center for Neurosciences Berlin, 10117 Berlin, Germany.
3. Humboldt-Universität zu Berlin, Faculty of Philosophy, Berlin School of Mind and Brain, Berlin, Germany.
4. Department of Psychiatry and Psychotherapy, University of Cologne, Medical Faculty, Cologne, Germany.
5. Univ. Grenoble Alpes, F-38000 Grenoble, France.
6. OpenMind Innovation, F-75008 Paris, France.
7. Laboratory for Clinical Neuroscience, Centre for Biomedical Technology, Universidad Politecnica de Madrid, Spain.
8. Department of Clinical and Movement Neurosciences, UCL Queen Square Institute of Neurology, London, UK.
9. National Hospital for Neurology and Neurosurgery, UCL Queen Square Institute of Neurology, London, UK.
10. Hospital Clínico San Carlos, Neurosurgery Department, Universidad Complutense de Madrid, Madrid, Spain
11. Department of Stereotactic and Functional Neurosurgery, University of Cologne, Cologne, Germany.

12. Inserm, U1216, Grenoble Institut des Neurosciences, F-38000 Grenoble, France.
13. Psychiatry Department, CHU Grenoble Alpes, F-38000 Grenoble, France.
14. Johanniter Hospital Oberhausen, EVKLN, Department of Psychiatry, Psychotherapy and Psychosomatics, Oberhausen, Germany.

Corresponding Author

Ningfei Li
Movement Disorders and Neuromodulation Unit, Department of Neurology, Charité – Universitätsmedizin Berlin (CCM), Charitéplatz 1, 10117 Berlin, Germany. E-mail: ningfei.li@charite.de

Keywords

Obsessive-Compulsive Disorder (OCD), Deep Brain Stimulation (DBS), Anterior Limb of the Internal Capsule (ALIC), Subthalamic Nucleus (STN), Connectome, Functional Connectivity

Word counts

Number of words in the abstract: 248
Number of words in the main text: 3998
Number of Figures: 6
Number of Tables: 2

Abstract

Background: Multiple deep brain stimulation (DBS) targets have been proposed for treating intractable obsessive-compulsive disorder (OCD). Here, we investigated whether stimulation effects of different target sites would be mediated by one common or several segregated functional brain networks.

Methods: Seeding from active electrodes of four patient cohorts (N = 50) with DBS to anterior limb of the internal capsule or subthalamic nucleus zones, optimal functional connectivity profiles for maximal Yale-Brown Obsessive-Compulsive Scale improvements were calculated and cross-validated in leave-one-cohort-out and leave-one-patient-out designs. Second, we derived optimal target-specific connectivity patterns to determine brain regions mutually predictive of clinical outcome for both targets and others that were predictive for either target alone. Functional connectivity was defined using resting state functional MRI data acquired in 1,000 healthy participants.

Results: Optimal functional connectivity profiles showed commonalities and differences between target sites, while cross-predictions of improvements remained robust across cohorts and targets, suggesting a shared network. Connectivity to anterior cingulate cortex, insula, and precuneus, among other regions, was predictive regardless of stimulation target. Regions with maximal connectivity to these commonly predictive areas included insula, superior frontal gyrus, anterior cingulate cortex and anterior thalamus, as well as the original stereotactic targets.

Conclusions: Pinpointing the network modulated by DBS for OCD from different target sites identified a set of brain regions to which DBS electrodes associated with optimal outcomes were functionally connected – regardless of target choice. On these grounds, we elucidate potential brain areas that could prospectively inform additional or alternative neuromodulation targets for OCD.

Introduction

For approximately 10% of obsessive-compulsive disorder (OCD) patients refractory to conventional first-line interventions (1), deep brain stimulation (DBS) and stereotactic ablation provide effective alternative treatment options (2,3).

Since the early times of stereotactic neurosurgery, disrupting dysfunctional networks has ranked prominently among treatment strategies for brain disorders (e.g., via *ansotomy* – or lesioning of the ansa lenticularis – as performed by Spiegel and Wycis or others in 1954 (5)). From as early as ~1888 on, an underlying rationale was to alleviate pathological communication between cerebral subsystems via their separation (4). Modern neuroimaging methods are now beginning to facilitate mapping such remote network-level effects in a more systematic and model-driven fashion (6–18). These more recent studies may confirm the impact of DBS on distributed pathological brain networks and allow anticipating essential network targets for maximized efficacy (19).

Severe forms of OCD have been termed *circuitopathies* (20,21), suggesting optimal treatment responses to result from rebalancing exactly the affected brain networks. Specifically, current views propose OCD symptoms to arise from i) excessive activity in direct over indirect cortico-striato-pallido-thalamo-cortical (CSTC) loops, and ii) abnormal frontostriatal connectivity (22–30). In this concept, the dACC, which mediates conflict processing between affective (orbitofrontal) and cognitive (dorsolateral prefrontal) inputs plays a central role (31). In case of OCD, an imbalance favoring limbic over associative loops leads to inappropriate dACC activity, inducing a pathological state of error/conflict signaling that may involve hyperdirect input to the associative/limbic STN (32).

While predominantly embedded within this circuitry, no definite agreement about one single optimal DBS target or network for OCD has yet been reached (33). Common targets include limbic/associative gray matter nuclei such as the anteromedial subthalamic nucleus (amSTN) (34–36), nucleus accumbens (NAcc) (37), or ventral striatum (VS)/ventral capsule (VC) (38). Other proposed targets include fronto-subcortical white-matter fiber bundles, such as the anterior limb of the internal capsule (ALIC) (39), bed nucleus of the stria terminalis (BNST) (40), inferior thalamic peduncle (ITP) (41,42), or ventral tegmental area projection pathway (VTApp; formerly termed superolateral medial forebrain bundle; slMFB) (43).

Critically, similar response rates (in terms of global obsessive-compulsive symptomatology) (2), along with anatomic juxtaposition between some of these targets may imply a unifying pathophysiological mechanism (44). Moreover, given stimulation spread, anatomical diversity of local neuronal and fiber distributions, slight targeting imprecisions, and the wide span of electrode contacts (between 6 and 21 mm across ventral and dorsal contact centers), on average, differences in target definition are often merely semantic (12). Broadly, most targets can be divided into an ALIC/striatum zone (including ALIC, BNST, VS/VC, and NAcc), and one at the junction between brainstem and forebrain (including amSTN and VTApp). We will thus use the terms ALIC-DBS and STN-DBS to describe these zones, unless otherwise specified.

Recently, clinical outcome following stimulation to either region was shown to be associated with optimal treatment outcome when the same specific white matter tract (passing through both areas) was modulated (12). Based on this tract, improvements could be predicted across DBS targets and independent datasets from different DBS centers (12). The tract traversed the ALIC focally, would macroscopically center around the frontopontine projection pathway (also termed *Arnold's bundle*), and may functionally comprise hyperdirect prefrontal input to STN and midbrain structures.

However, structural network analyses (such as conducted with diffusion-MRI based tractography, dMRI) bear the short-coming of neglecting indirect connections across distributed functional (whole-brain) networks. Here, we hence build on a previous dMRI study (12) to investigate differences and commonalities of *functional* networks associated with either OCD target category. Based on resting-state functional MRI (rs-fMRI) data acquired across 1,000 healthy subjects, we first identify optimal networks in relation to clinical outcome across the whole patient group and cross-validate these via leave-one-cohort-out and leave-one-patient-out designs. Crucially, functional connectivity is modeled via rs-fMRI data from healthy subjects, while seed regions are obtained from patients. Second, we inspect specificity of and differences in optimal networks between STN vs. ALIC cohorts. We then compare a connectivity profile predictive for *both* targets (i.e., an *agreement map*) to a full-cohort map in terms of predictive utility. Considering the agreement map's superior ability in explaining outcome variance, it might represent the set of connections a DBS electrode should optimally display – regardless of target choice. Finally, we raise the question: Which voxels in the brain maximally display exactly this set of connections? We therefore *invert* the agreement map to identify brain regions with a connectivity profile maximally similar to this map and validate it against a meta-analytic connectivity pattern functionally linked to OCD. This step intends elucidating and confirming stimulation targets – or network *sweet-spots* – with connectivity profiles most strongly resembling the agreement map.

Methods and Materials

Patient cohort

Detailed methodological descriptions can be found in supplemental material. Analyses were based on retrospective data of the same 50 OCD patients from four centers as described in (12), comprising *Cologne* (N = 22 ALIC-DBS patients), *Grenoble* (N = 14 STN-DBS patients), *Madrid* (N = 8 NAcc-DBS patients), and *London* cohorts (N = 6 patients with bilateral electrodes targeting both STN and ALIC). Since, as shown in (12), placements of NAcc electrodes (Madrid sample) on average were similar to the ones of ALIC electrodes (Cologne and London samples), we subsumed NAcc electrodes conforming to an ALIC zone going forward. For more comprehensive clinical descriptions, see **Table 1** (largely adopted from (12)).

Pre- and postoperative OCD symptom severity was assessed on the Yale-Brown Obsessive-Compulsive Scale (Y-BOCS) (45). Information on imaging data, electrode localization and volumes of tissue activated (VTAs) estimation performed in Lead-DBS software (http://www.lead-dbs.org) (46,47) is detailed in supplements.

DBS connectivity analysis

Functional connectivity analyses were based on a normative functional connectome, calculated from rs-fMRI scans of 1,000 healthy subjects (48) acquired within the Brain Genomics Superstruct Project (https://dataverse.harvard.edu/dataverse/GSP; (49)). Similarly to previous studies (6,9), voxel-wise correlations between time-series of voxels inside each bilateral VTA and of remaining whole-brain voxels were calculated per OCD patient, averaged across the normative sample, and Fisher-z-transformed (**Figure 1 A**). On a voxel-by-voxel basis, the resulting, patient-specific fingerprints were correlated with Y-BOCS improvements across patients to generate an *R-map model*

of “optimal” connectivity profiles for maximal Y-BOCS improvement (**Figure 1 B**). This R-map models regions to which DBS electrodes ideally should (red regions, **Figure 1 B**) or should not be connected (blue regions) to maximize Y-BOCS improvement. More details are displayed in the supplemental material.

If the R-map itself represents a model of optimal connectivity, higher similarity of individual fingerprints to the model would link to better clinical outcome. To test this assumption, spatial similarity metrics between individual *fingerprints* and the *R-map* were used to predict clinical improvements of *novel* patients (**Figure 1 C**). If not otherwise specified, circularity of analyses was avoided by calculating R-maps on the basis of *one* part of the sample to predict outcomes in a *different* part, specifically using i) leave-one-cohort-out, and ii) leave-one-patient out designs.

Based on *target-specific* R-maps (i.e., one distinct map for ALIC and STN zones, respectively), an *agreement map* was derived with the aim of quantifying overlaps of optimal connectivity across DBS targets. R-maps from these two cohorts were multiplied with each other while retaining only voxels that were either positive or negative simultaneously in *both* maps (**Figure 1 D**). Voxels negative on both maps were kept negative despite their (absolute) values being multiplied.

To identify subcortical target *sweet spots* that could define optimal neuromodulation sites, we calculated which voxels throughout the whole brain had connectivity profiles that were maximally similar to the resulting agreement map. Since the agreement map itself included subcortical targets, we first restricted its profile to cortical (and cerebellar) regions (this step did not alter results; see supplements). Using a voxel-wise precomputed connectome of the same rs-fMRI dataset (49), we then identified brain-wide voxels with a cortical connectivity profile most similar to the (cortical) agreement map, termed *inverted map* (**Figure 1 D; Figure 6**). These regions

exhibit a connectivity profile that could be considered “optimal” based on data from cohorts operated with two different DBS targets.

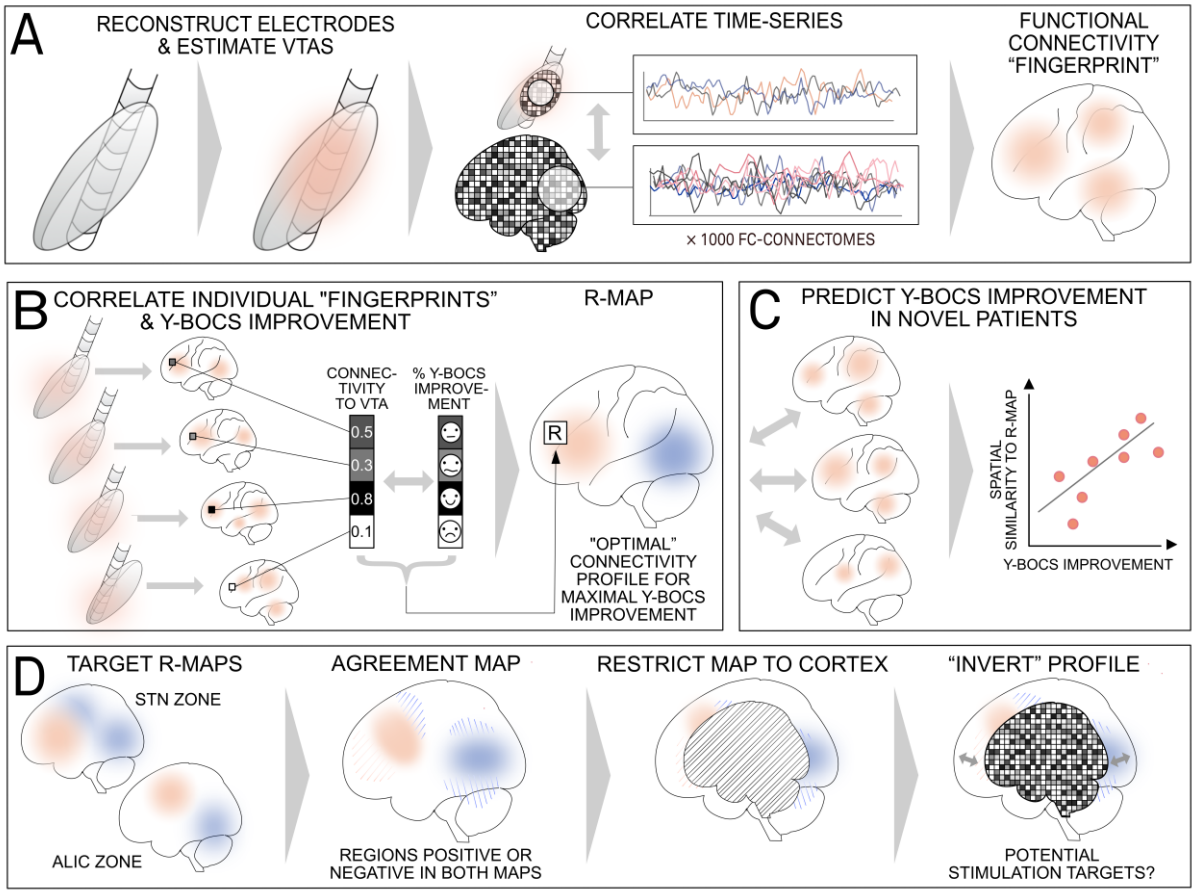

Figure 1. **Schematic of methodological pipeline.** (**A**) First, deep brain stimulation (DBS) electrode localizations were reconstructed in stereotactic standard space, and volumes of tissue activated (VTAs) (red) were estimated based on individual stimulation parameters. Using a normative high-resolution resting-state functional MRI (rs-fMRI) connectome derived from data of the Brain Genomics Superstruct Project (Holmes et al., 2015), average time-series of voxels within bilateral VTAs and of every other whole-brain voxel were correlated. Per patient, this analysis was performed 1,000 times via data of each subject in the normative sample (N = 1,000 healthy subjects) and subsequently averaged, resulting in one functional connectivity fingerprint for each patient. (**B**) Depending on respective DBS electrode placement and individual stimulation parameter settings, these fingerprints varied between patients. Voxel-wise correlation between patients’ fingerprints and individual Yale-Brown Obsessive-Compulsive Scale (Y-BOCS) change scores resulted in an R-map, whose spatial distribution by itself estimated an “optimal” connectivity profile of DBS electrodes. Hence, voxels with positive correlations (red) depict areas to which connectivity seeding from the VTA were associated with beneficial outcome, and vice versa for anticorrelated voxels (blue). (**C**) Probing this R-map as a predictive model, clinical outcomes of

novel patients (not used to define the model) were estimated based on spatial correlation (i.e., similarity) between the R-map and each novel patient's functional connectivity fingerprint. (**D**) For each of the two target zones (anterior limb of the internal capsule, ALIC, and subthalamic nucleus, STN), one separate R-map model was estimated. Based on both, an agreement map was calculated by discarding voxels in which the signs on both R-maps were conflicting and multiplying their absolute values when signs were in agreement. The resulting map may constitute an optimal connectivity map that applies for both target sites. Finally, we aimed to determine which regions in the brain were maximally connected to this map. To do so, connectivity profiles of every single voxel were compared (by spatial correlation) to the cortical surface of the agreement map. The resulting "inverted" map peaked at regions maximally connected to the agreement map. FC, functional connectivity.

For correlation analyses comparing predicted and empirical improvements, p-values were obtained via Monte-Carlo random permutations (×1,000). This procedure is free from assumptions about distributions (i.e., Student t for R-values), which are typically violated in small sample sizes. Scatterplots were visualized with 95% confidence bounds (gray or light-red areas).

Finally, we validated our inverted connectivity profile against a meta-analytic brain network functionally implicated in OCD. Specifically, by computing a voxel-wise spatial correlation coefficient across the brain, we tested how this inverted map compared to a pattern of activations linked to the search term "obsessive compulsive" entered into NeuroSynth (www.neurosynth.org; term-based meta-analyses) (50). This search engine automatically derives meta-analytic whole-brain activation maps based on text mining across neuroscientific publications to avoid biased study selection.

Results

Age, as well as relative pre- to post-surgical Y-BOCS improvements were comparable across centers (see **Table 1** for details). Electrode localization confirmed accurate placement in both ALIC and STN target zone cohorts (**Figure 2**).

Table 1: Patient demographic details and clinical results of the four cohorts.

	ALIC-DBS Cohort (Mean ± SD)	STN-DBS Cohort (Mean ± SD)	NAcc-DBS Cohort (Mean ± SD)	Combined DBS Cohort (Mean ± SD)
Center	University Hospital Cologne	University Hospital Grenoble	Hospital Clínico San Carlos Madrid	University Hospital London
Reference(s)	(7,84)	(116)	(85)	(70)
N patients (females)	22 (12)	14 (9)	8 (4)	6 (1)
N electrodes	44	28	16	24
Age	41.7 ± 20.5	41 ± 9	35.3 ± 10.4	45.5 ± 10.5
Y-BOCS baseline	31.3 ± 4.4	33.4 ± 3.7	30 ± 7.75	36.2 ± 1.8
Y-BOCS after DBS	20.7 ± 7.7 *(12 months postop)*	19.6 ± 10.6 *(12 months postop)*	14.75 ± 7.2 *(3 months postop of best contact)*	14.3 ± 4.1 *(optimized phase in* (70)*)*
Absolute Y-BOCS improvement	9.6 ± 6.5	13.8 ± 10.8	15.1 ± 9.6	21.83 ± 5.7
%-Y-BOCS improvement	31.0 ± 20.5 %	41.2 ± 31.7 %	47.8 ± 23	60.2 ± 12.7 %

Abbreviations: **ALIC**, anterior limb of the internal capsule; **DBS**, deep brain stimulation; **NAcc**, nucleus accumbens; **SD**, standard deviation; **STN**, subthalamic nucleus; **Y-BOCS**, Yale-Brown Obsessive-Compulsive Scale.

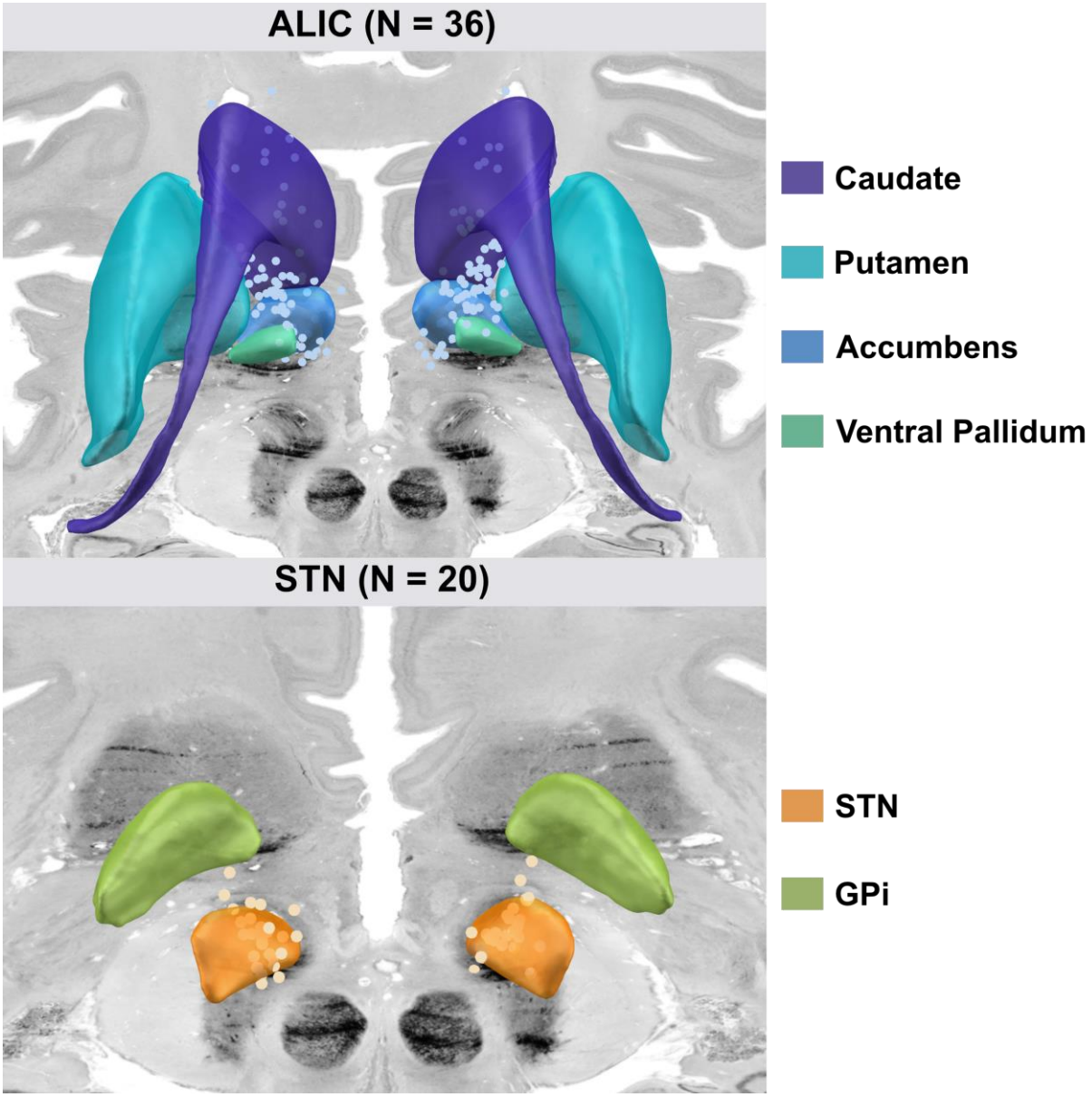

Figure 2. **Overview of lead electrode placement.** Active electrode contacts from the ALIC and STN cohorts are shown. Note that patients from the Madrid cohort were implanted with a Medtronic 3391 type lead which spans across 21 mm from ventral to dorsal contact centers, hence the larger spread of contacts extending to dorsal in this cohort (top panel). Subcortical structures defined by CIT-168 Reinforcement Learning atlas (114) (anterior limb of the internal capsule zone, ALIC) and DISTAL atlas (115) (subthalamic nucleus zone, STN), with coronal and axial planes of the BigBrain template (116) as background. GPi, globus pallidus internus.

First, an R-map model accounting for the overall effect *regardless* of DBS target was calculated based on the full patient cohort. Then, we cross-validated this model using leave-one-patient-out (**Figure 3** bottom left), as well as leave-one-cohort-out designs (**Figure 3** bottom right). Leaving one cohort out did not largely affect the spatial R-map

configuration. The four maps were used to cross-predict variance in clinical improvements of the left-out cohort via spatial correlation between left-out patients' connectivity fingerprints and the respective R-map model (**Figure 3** bottom right side; R = 0.31, p = 0.005). The R-map calculated on all patients (see **Figure 4** bottom left) associated positive connectivity between electrodes and insula as well as cingulate cortex most prominently with clinical response. Notably, instead of showing how the two targets involved the *exact* same network, our aim here was to investigate both across-target commonalities *and* differences. Notwithstanding robust findings across cohorts, we must emphasize that higher numbers of ALIC-DBS as STN-DBS patients may have driven effects. The following analyses investigated this further.

Apart from robustness of an *overall* network predictive of clinical improvement across cohorts (**Figure 3**), we were also interested in *differences* between the two target zones when analyzed separately. Thus, R-map models were derived from two sub-sets of the full sample split based on target region (ALIC vs. STN zone; **Figure 4**). While connectivity to some brain regions was associated with optimal clinical outcomes regardless of DBS target (such as anticorrelations to sensorimotor cortex or positive connections to striatum, insula and specific cingulate regions), others did not overlap. For instance, regions such as the orbitofrontal cortex (OFC) were highlighted by the STN but not the ALIC R-map, and regions such as the supramarginal gyrus showed the opposite pattern.

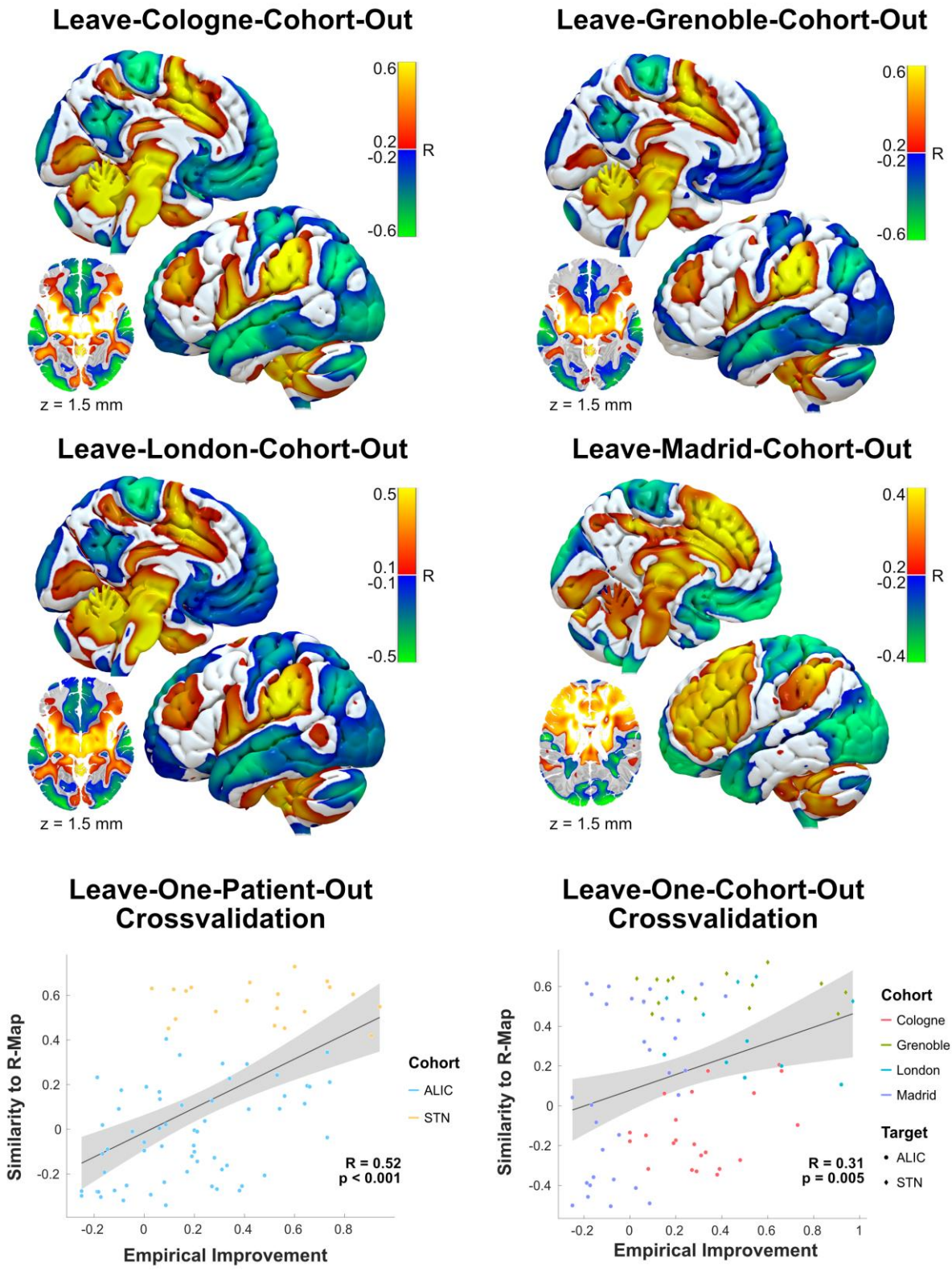

Figure 3. **Leave-One-Patient-Out and Leave-One-Cohort-Out cross-validations of the R-map model.** Patients were divided by DBS centers into four cohorts. The first four panels show correlation maps between functional connectivity fingerprints (seeding from bilateral VTAs in each patient to the rest of the brain) and clinical improvements. Maps are displayed in form of brain surface overlays together with an additional axial slice at z = 1.5 mm, with yellow to red colormap indicating positive R-values and blue to green colormap indicating negative R-values. Results of the leave-one-patient-out cross-validation are shown on the bottom left panel, while results of the

leave-one-cohort-out cross-validation are presented on the bottom right panel. Here, each map was calculated on data of three out of the four cohorts and used to cross-predict outcomes in patients from the respectively left-out cohort. Axial planes show the BigBrain template (116) as background. ALIC, anterior limb of the internal capsule zone; STN, subthalamic nucleus zone.

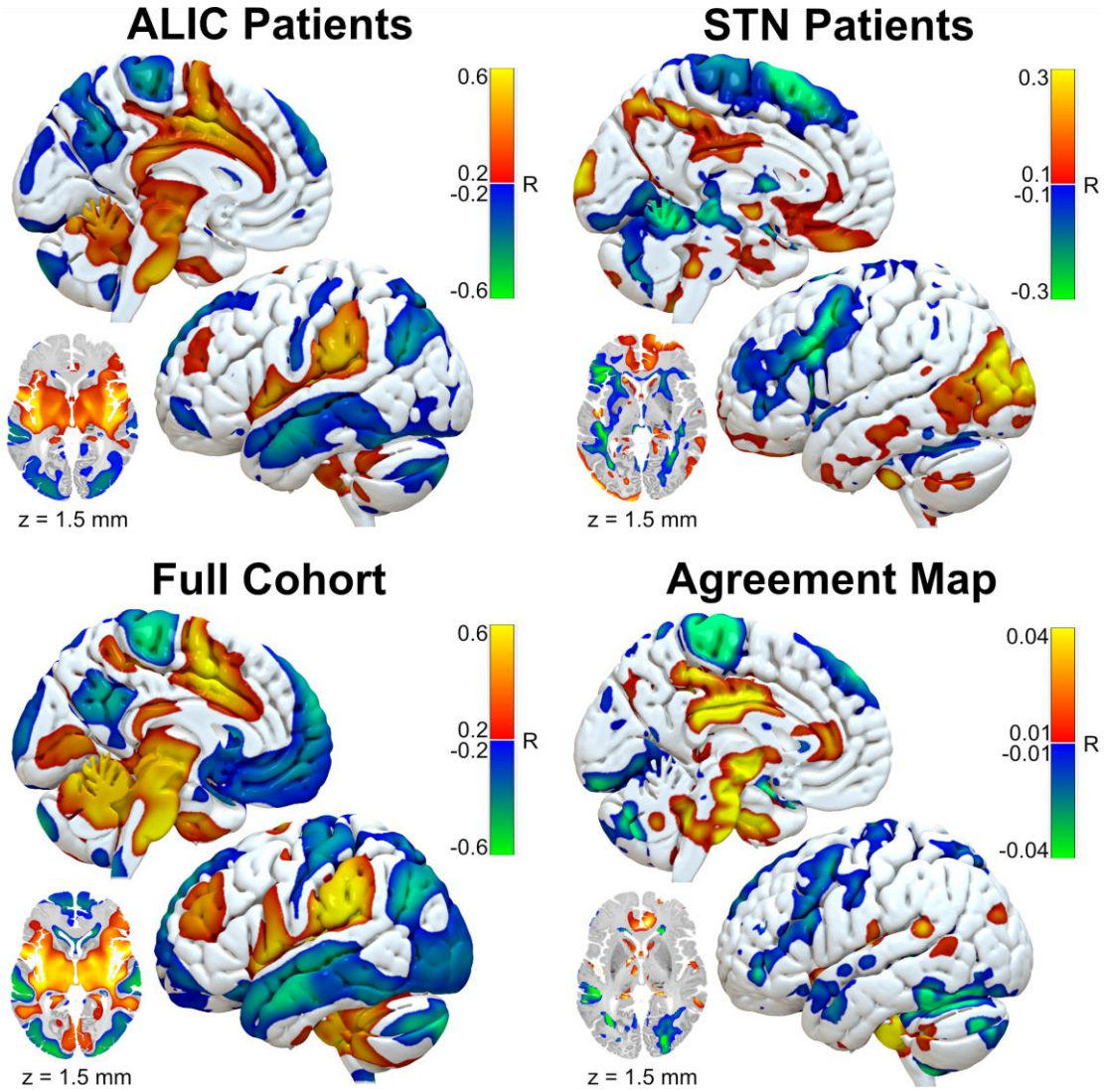

Figure 4. **Functional connectivity profile of cohorts divided by target zone.** R-maps were calculated by correlating functional connectivity fingerprints (seeding from bilateral VTAs in each patient to the rest of the brain) and clinical improvements. R-maps from anterior limb of the internal capsule (ALIC; top left) and subthalamic nucleus (STN; top right) zone cohorts separately, from full cohort combined (bottom left), and agreement map based on the ALIC and STN maps (bottom right) are displayed. Maps are shown as brain surface overlays along with an additional axial slice at z = 1.5 mm, with yellow to red colormap indicating positive R-values and blue to green colormap indicating negative R-values. Anatomical regions of these results are reported in supplementary Table S1. Axial planes show the BigBrain template (116) as background.

We hypothesized that areas convergently identified by both maps could be more specific to the true DBS effect (while others could have resulted from indirect connections revealed in rs-fMRI connectivity analyses or spurious correlations). Hence, in addition, an agreement connectivity map between ALIC-DBS and STN-DBS cohorts was calculated by rejecting areas without agreement across the two maps (**Figure 4** lower right). Of note, while the full cohort map highlighted the dACC, the STN map was only mildly positively correlated here (but correlated to other ACC regions). As a consequence of coefficient multiplications, the agreement map almost showed a gap in dACC but highlighted rostral and posterior ACC.

To test whether this approach could improve utility of models, we computed the amount of variance explained using either the full-cohort R-map or the aforementioned *agreement map* (**Figure 5**). While the full-cohort R-map accounted for ~24% of the variance in clinical improvements ($R = 0.49$, $p < 1e\text{-}5$), the agreement map did so for ~32% ($R = 0.57$, $p < 1e\text{-}7$). In the ALIC cohort, the full map explained ~18% ($R = 0.43$, $p < 1e\text{-}3$), and the agreement map ~27% ($R = 0.52$, $p < 1e\text{-}4$) of variance. In the STN cohort, neither map accounted for a significant amount of variance in pre- to postoperative Y-BOCS change, but the association was stronger in the agreement map ($R = -0.07$ vs. $R = 0.31$). We must emphasize that differences in predictive utility were not significant ($p = 0.127$, 0.211, 0.095 for combined, ALIC and STN targets, respectively) and are meant as direct head-to-head comparisons of each map's utility that at best may lead to anecdotical evidence.

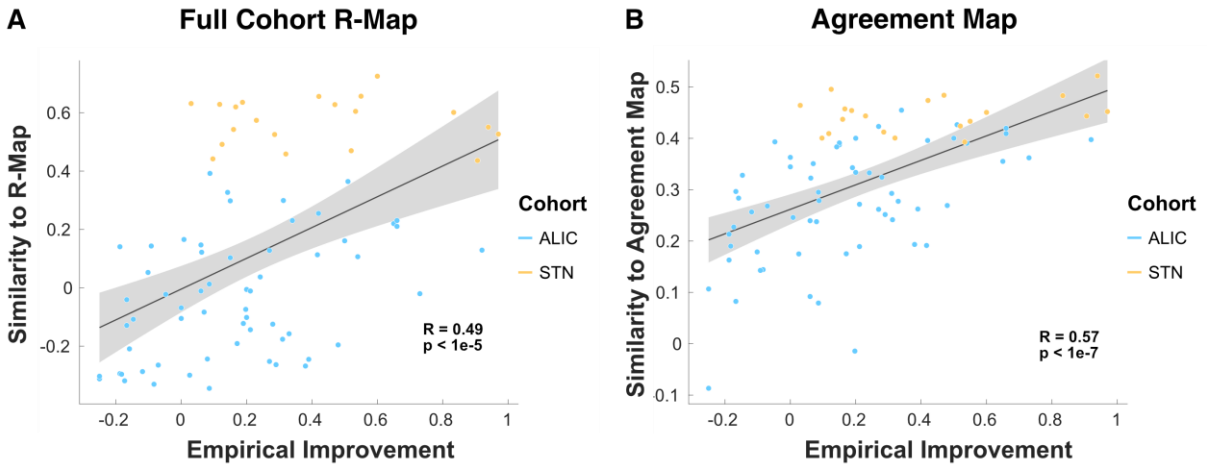

Figure 5. **Amount of variance in clinical improvement that could be explained using the full cohort R-map (left) vs. agreement map (right) models.** (**A**) Correlation between clinical improvement and spatial similarities between network fingerprints and the R-map model calculated across all patients of the full cohort. (**B**) Correlation between clinical improvement and spatial similarities between network fingerprints and the agreement map model. Please note that the aim of the figure is to directly compare the full cohort R-map model with the agreement R-map model. Correlations shown in this figure do not represent actual (out-of-sample) predictions since all data points were used to calculate both models. ALIC, anterior limb of the internal capsule; STN, subthalamic nucleus.

By integrating the agreement R-map with a preprocessed version of the functional connectome (48), we *"inverted"* its connectivity profile to find regions with connectivity profiles of strongest similarity to this map (**Figure 6**). For each brain voxel, this map estimated via spatial correlation *how similar* its connectivity profile was to the agreement map. If the agreement pattern indeed consisted of an optimal across-target connectivity profile of effective DBS, the inverted map would highlight regions *exhibiting* exactly this optimal connectivity profile. The resulting *inverted* map comprised the two DBS targets of study (ALIC and STN). Peak voxels resided at similar locations (~2 mm distance) to average active stimulation contacts in both regions (see **Table 2**; ALIC: DBS stimulation site: ±10.73, 9.20, -2.48 mm; peak voxel on inverted map: ±11.46, 7.36, -2.37 mm; STN: DBS stimulation site: ±10.04, -11.52, -7.84 mm; peak voxel on inverted map: ±9.40, -10.01, -6.91 mm). However, the inverted map also

highlighted common cortical targets of transcranial magnetic stimulation (TMS; e.g., dACC, OFC, and dlPFC) or stereotactic ablation (e.g., the ACC) for treating OCD. The most prominent anatomical regions in R-maps for ALIC and STN cohorts, as well as agreement and inverted maps are summarized in supplementary **Table S1**.

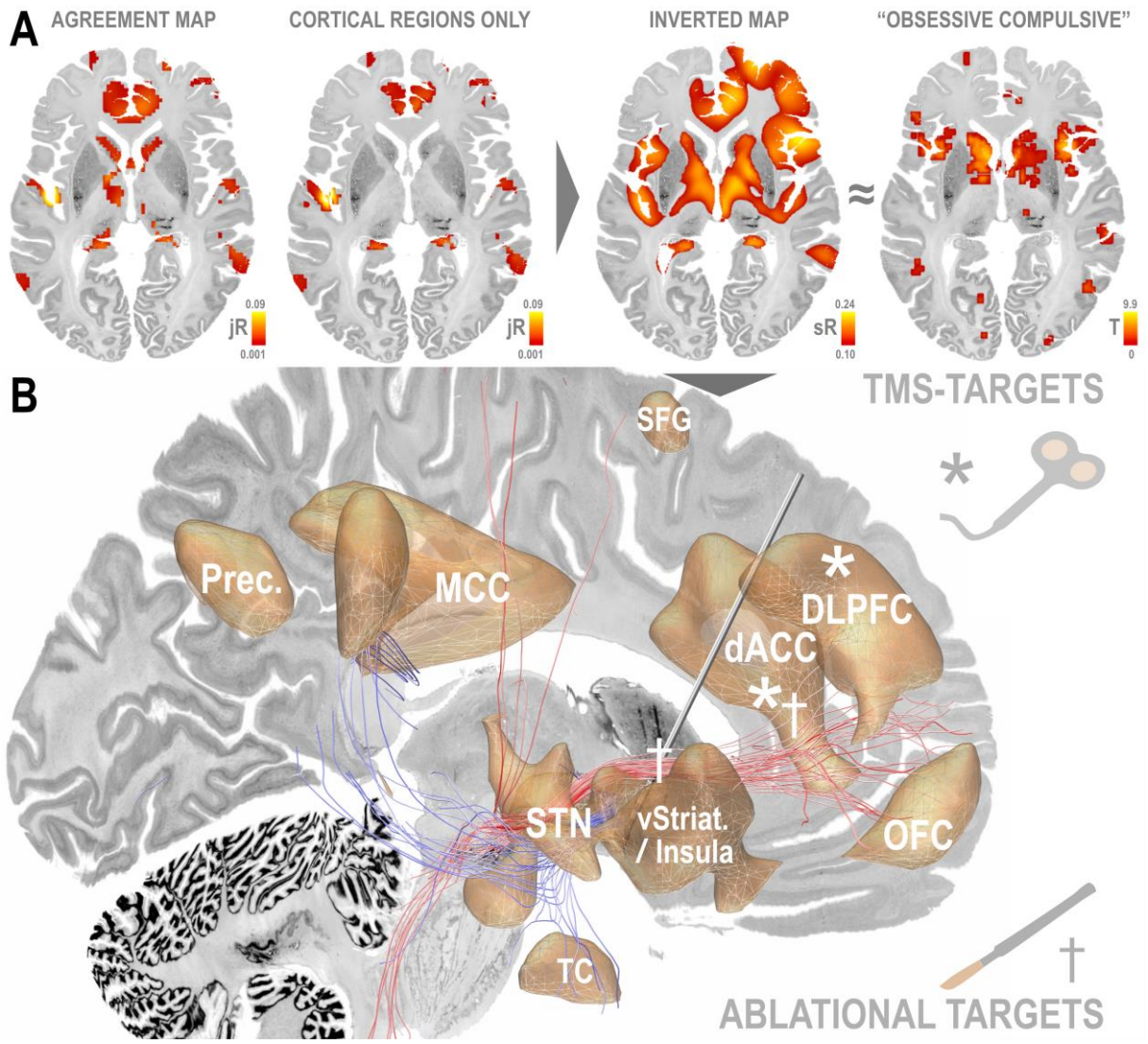

Figure 6. **"Inversion" of the agreement map to estimate potentially optimal stimulation target regions.** (**A**) The agreement map (regions a connection to which was associated with clinical improvements in both anterior limb of the internal capsule, ALIC, and subthalamic nucleus, STN, zone DBS cohorts, expressed as multiplied R-values across the two maps, jR) was restricted to cortical regions to avoid that subcortical connectivity regions would bias subsequent analyses. Based on a preprocessed version of the N = 1,000 functional connectome, each brain voxel's connectivity profile was spatially compared to the cortical agreement map (by means of spatial correlation, sR). This inverted map identifies which brain regions are maximally connected to the

agreement map and showed strong similarity with automated meta-analyses for the term “obsessive compulsive” (red-yellow colormap; R = 0.30, p < 1e-17; obtained from neurosynth.org). (**B**) The inverted map – as a potential set of neuromodulation targets – is shown in 3D in synopsis with an ALIC-DBS electrode, the optimal structural connectivity target published on the same cohort of patients (12), as well as with remarks about transcranial magnetic stimulation (TMS) and lesioning targets that showed efficacy for treatment of obsessive-compulsive disorder, in the past. The parasagittal plane represents a slice from the Bigbrain dataset (116). dACC, dorsal anterior cingulate cortex; dlPFC, dorsolateral prefrontal cortex; MCC, medial cingulate cortex; OFC, orbitofrontal cortex; Prec., precuneus; SFG, superior frontal gyrus; TC, temporal cortex; vStriat., ventral striatum.

Table 2: Peaks of inverted map vs. average DBS stimulation sites in ALIC vs. STN DBS cohorts.

	Average Coordinate Active DBS contacts [mm]	Peak within structure on Inverted Map [mm]	Euclidean Distance [mm]
ALIC			
Left hemisphere	-11.02/8.91/-2.41	-10.81/5.78/-2.94	3.2
Right hemisphere	10.45/9.28/-2.54	12.03/8.93/-1.84	1.8
Average coordinate	**±10.73/9.20/-2.48**	**±11.46/7.36/-2.37**	**1.9**
STN			
Left hemisphere	-9.97/-11.84/-7.99	-9.41/-10.23/-7.37	1.8
Right hemisphere	10.10/-11.20/-7.64	9.40/-9.78/-6.41	2.0
Average coordinate	**±10.04/-11.52/-7.84**	**±9.40/-10.01/-6.91**	**1.9**

Abbreviations: **ALIC**, anterior limb of the internal capsule; **DBS**, deep brain stimulation; **STN**, subthalamic nucleus. Note that average coordinates were calculated using nonlinear flips established within Lead-DBS (due to use of an asymmetric, more realistic MNI template).

An additional – crucially circular – analysis was amended to test a suggested technique for potential future independent comparisons on out-of-sample data. Namely, we calculated weighted overlaps between each patient’s VTA and the inverted map. Results of this analysis significantly correlated with clinical improvements (R = 0.54, p < 1e-6).

Last, an automated meta-analytic activation pattern derived from 98 studies, detected via NeuroSynth ((50); www.neurosynth.org; uniformity tests) for the term *“obsessive compulsive”*, showed striking similarity to the inverted map in terms of spatial correlation strength (**Figure 6**; $R = 0.30$, $p < 1e\text{-}17$).

Discussion

Four major points can be drawn from this study: First, an overall optimal functional connectivity model yielded robust predictions of Y-BOCS outcomes across OCD cohorts both in a leave-one-cohort-out and a leave-one-patient-out fashion, on group-level. In other words, variance in clinical outcomes could be cross-predicted across the two DBS targets (ALIC and STN zones) and four DBS centers based on normative rs-fMRI profiles seeding from patient-specific, active DBS electrode contacts. Second, while target-specific optimal functional connectivity profiles (ALIC vs. STN) differed in several brain regions, a considerable set of areas was shared between targets. Third, when restricting our model to these regions (in form of an agreement map), the predictive utility for both cohorts increased. Hence, by pinpointing the optimal network model from two separate nodes (i.e., via different DBS targets), the resulting model might have become more robust and specific. Last, inverting the agreement map revealed potential targets for neuromodulation in OCD. Naturally, this included the two DBS targets of study (ALIC and STN), with ALIC also a known target for stereotactic ablation, but also common cortical targets for TMS (such as the dACC, OFC, and dlPFC) or stereotactic ablation (such as the dACC).

Common circuitry of effective DBS in OCD

First and foremost, the potential across-target neuromodulation *sweet spots* identified here via agreement map inversion integrate with important aspects of the hypothesized etiology of obsessive-compulsive symptoms, involving aberrant frontosubcortical limbic projections (23,24,27,29). The STN receives direct cortical input from most if not all regions of the PFC: After originating from specific prefrontal structures, its associative-limbic domains traverse parts of the ALIC and send axon collaterals to the

amSTN and other midbrain structures (51,52). Among these hyperdirect input areas, the dACC plays a prominent role for OCD pathophysiology (31,51,53).

Crucially, this hyperdirect trajectory largely matched the structural connectivity profile associated with optimal ALIC-DBS (7,12,54,55) and STN-DBS (12) outcomes for OCD. Extending these findings, the inverted pattern in the present study revealed optimal connectivity of agreement profiles between DBS electrodes – irrespective of target choice – with the ACC. These convergent results may hint at a fundamental, overarching network substrate of successful DBS in OCD. However, direct input from dACC to amSTN may be one link (or *edge*) in a network (or *circuitopathy*) consisting of additional brain regions (or *nodes*).

Functionally, the dACC consistently links to OCD symptom severity across resting-state and symptom-provocation studies, with reductions in excessive dACC activation following successful interventions (56–64). According to the *control signal theory of dACC dysfunction* (31), the dACC integrates input from other prefrontal structures such as the OFC, ventromedial PFC (vmPFC), and dlPFC involved in executive planning in response to unpleasant stimuli and/or *conflict* (compare with regions identified here; **Figure 6**). The dACC then emits a control signal to effectors such as the pre-supplementary motor area (pre-SMA) and SMA. Unlike in healthy individuals, in OCD, conflict resolution does not lead to normalized dACC activity and concurrent control signal extinction, potentially due to ongoing OFC or striatal activation. Instead, a vicious circle of repetitive behaviors (compulsions), accompanied by emotional distress (obsessions) follows. In line with this, recalibrating OCD-related dACC hyperactivity may thus provide a functional avenue for interrupting the maladaptive control signals chain reaction, restoring cognitive control and goal-directed behavior.

Indeed, OCD-DBS likely mirrors effects comparable to a long-standing tradition of neurosurgical approaches, which disrupt frontostriatal and/or frontosubthalamic connectivity to rebalance OCD-related dACC hyperactivity. While disconnecting white-matter bundles via bilateral *capsulotomy* led to successful OCD symptom alleviation as early as in the 1950s (65) – with new traction gained via gamma-knife surgeries or MR-guided focused ultrasound (66) – the long-term therapeutic efficacy of surgical dACC lesioning (*cingulotomy*) (67,68) has since been extensively confirmed. Similarly, efficacy of DBS may rely on normalizing frontostriatal connectivity in treatment-refractory OCD patients (37). Moreover, efficacious DBS sites targeted to the amSTN connected mainly to the dACC – alongside the lateral OFC and dlPFC (69). Li et al. expanded on this finding in elucidating the association of these connections with clinical improvements (12). Beyond that, positron emission tomography studies similarly indicated decreased prefrontal metabolism in OCD following both STN-DBS (70) and ALIC-DBS (71). Finally, the dACC (and dlPFC) count among the few noninvasive neuromodulation targets for OCD approved by the US Food and Drug Administration (72,73).

Beyond the classical CSTC pathway, the inverted across-target circuitry of effective DBS complements emerging evidence on more widely distributed dysfunctional brain systems (e.g., limbic, salience, or default mode networks) contributing to OCD pathogenesis (21,26,74). For instance, not only does the insula functionally connect to the CSTC circuitry (75,76), but compared to healthy controls, OCD patients also consistently display altered, task-related insular activation (77–79). Accordingly, a recent study showed that DBS to the ALIC increased the impact of vmPFC onto the amygdala, decreasing amygdalar impact onto the insula (80). Switching DBS off reversed this pattern drastically, along with sudden depressive or anxious exacerbations. Still, it remains to be established whether such nodes could

become involved in effective therapy of obsessions or compulsions per se rather than in that of OCD comorbidities (81).

Apart from optimal *post*-surgical DBS electrode connectivity, other amounts of clinical outcome variance may be explained by patient selection – since not all patients show uniform symptom profiles and may thus differentially respond to treatment. This raises a need for preoperative baseline predictors of response to DBS in OCD (2,82,83). Here, the most impaired patients (London cohort), on group level, appeared to benefit most from the intervention. However, statistical tests of a potential interaction may be biased in this particular cohort due to the retrospective study character, small sample size (N = 6) and patient-wise implantation of four electrodes, increasing stochastic likelihood of hitting a specific beneficial network. So far, no study has identified OCD symptom severity as a reliable candidate marker (2,83).

Target-specific circuitry

Beyond an *agreement* set of optimal connections across the two DBS targets, our target-*specific* models pointed out that, in addition, each may modulate separate networks. Such target-specific therapeutic networks may potentially be harnessed for tailoring treatment strategies to different disease subtypes or symptom domains (44,84,85). In other words, while both ALIC- and STN-targets may effectively reduce obsessive-compulsive symptoms registered by the Y-BOCS, each may complementarily lead to symptom changes across other domains – conceivably as a result of co-modulating target-specific networks.

Initial evidence indeed points towards behaviorally selective, target-specific DBS effectiveness sustained by differential OCD networks. In a prospective clinical study, ALIC-DBS preferentially improved depressive symptoms (potentially mediated via connectivity to the medial OFC), whereas amSTN-DBS selectively ameliorated

cognitive flexibility (potentially mediated via connectivity to the lateral OFC, dACC, and dlPFC) (69). Similarly, immediate improvements in mood and anxiety followed NAcc-DBS even in non-responders (86), while specific effects of STN-DBS on Y-BOCS outcome (but not on depression, anxiety, or other neuropsychological symptoms) were observed (36). Pertaining to specific OCD subtypes, refractoriness to NAcc-DBS was shown for perfectionism, hoarding, or symmetry (86). Still, since psychiatric DBS studies often rely on small samples, follow-up investigations should confirm the concept of symptom-specific substrates in OCD – and the one of shared network topologies.

The proposed unifying theory could henceforth – after sufficient prospective validation and replication via patient-specific connectomes – contribute to advancements in DBS programming, inform noninvasive stimulation targets (87), or add to a harmonized understanding of effective neuromodulation for OCD in a broader sense (88,89).

Limitations

There are several limitations to this study. First, the retrospective design warrants careful interpretation and prospective validation of interventional outcomes. Nevertheless, pooling a large sample allowed testing for robustness of effects across DBS centers and surgeons.

Second, non-linearly warping electrode sites into template space inevitably introduces inaccuracies. We sought to maximally counteract this bias by use of a state-of-the-art neuroimaging pipeline that includes brain-shift correction and subcortical refinement (47). Furthermore, we applied multispectral normalization, with an accuracy close to manual expert delineation as demonstrated by two independent groups (90,91), as well as electrophysiologically confirmed (92–98), phantom-validated

electrode localization methods (99). Crucially, results of each processing step underwent meticulous inspection and manual refinement by an expert user.

Third, the finite element VTA model applied in our analyses as well as the very *concept* of binarized E-field thresholding in general, are based on approximations that cannot truthfully incorporate every aspect of interactions between electrical current and neural tissue (100,101). While the approach applied here may represent a valid – albeit simplified – approximation (102), future studies may benefit from exploring more advanced concepts (101,103,104).

Fourth, estimates of therapeutic connectivity seeding from DBS electrodes in individual patients were based on normative connectomes. This concept has been widely applied in DBS, compared with individualized connectivity in Parkinson's Disease (105) or OCD (7), and may increase signal-to-noise ratios (85,106,107). However, its limited ability of accounting for patient-specific differences renders our study into a "broad lens view" on the brain, with a need for replication via individualized rs-fMRI data (108). Nevertheless, normative connectome-based models may represent first-order approximations of DBS network effects (6,9,11,12,109–111). Moreover, first proposed models have been prospectively validated by groups world-wide, underscoring reproducibility and clinical utility (54,105) (55,112). Importantly, despite group-level significance, results should not guide surgical targeting or DBS programming without thorough replication and refinement.

Last, although widely accepted as an interventional assessment in OCD and thus facilitating across-study comparisons (113), the explanatory value accessible via the Y-BOCS summary score is naturally limited to the effect of DBS onto global obsessive-compulsive symptomatology. While unfortunately, more comprehensive

neuropsychological assessments were unavailable, investigating postoperative network changes along different symptom axes represents a valuable future avenue.

Conclusions

In summary, we identify functional connectivity correlates of effective OCD-DBS in form of a distributed brain network, highlighting *differences* but also *commonalities* between ALIC and STN target zones. The distinctive *target-specific* connectivity features may point toward behaviorally selective therapeutic circuitries. Yet, fundamental across-target overlap allowed for significance in leave-one-cohort-out and leave-one-patient-out designs. Furthermore, a set of *agreement regions* outperformed a full-cohort model in terms of predictive utility for clinical improvements in both targets. Finally, we elucidate brain-wide regions exhibiting the most optimal connectivity profile as potential candidate targets for successful neuromodulation in OCD.

Acknowledgements

This work was supported by the Deutsche Forschungsgemeinschaft (DFG, German Research Foundation): Emmy Noether Stipend 410169619 to AH, Project-ID 424778381 – TRR 295 to AH and AAK, KFO 219 to JK. AH was further supported by Deutsches Zentrum für Luft- und Raumfahrt (DynaSti grant within the EU Joint Programme Neurodegenerative Disease Research, JPND). BH received funding via a scholarship from the Einstein Center for Neurosciences Berlin throughout this study. Computation has been performed on the HPC for Research cluster of the Berlin Institute of Health. To calculate normative stimulation-dependent connectivity, publicly available data from the Brain Genomics Superstruct Project (https://dataverse.harvard.edu/dataverse/GSP) were employed.

Disclosures

SC is consultant for Medtronic, Boston Scientific and Zimmer Biomet. MP has received honoraria for lecturing from the Movement Disorder Society, Medtronic, research support from Boston Scientific. JK has received financial support for investigator-initiated trials from Medtronic. AAK reports personal fees and non-financial support from Medtronic, personal fees from Boston Scientific, grants and personal fees from Abbott outside the submitted work. AH reports lecture fees for Medtronic and Boston Scientific. NL, BH, JCB, AK, ST, HA, BA-F, BS, JAB, LZ, EJ, and VVV have nothing to disclose.

References

1. Denys D (2006): Pharmacotherapy of Obsessive-compulsive Disorder and Obsessive-Compulsive Spectrum Disorders. *Psychiatric Clinics of North America* 29: 553–584.

2. Alonso P, Cuadras D, Gabriëls L, Denys D, Goodman W, Greenberg BD, *et al.* (2015): Deep Brain Stimulation for Obsessive-Compulsive Disorder: A Meta-Analysis of Treatment Outcome and Predictors of Response. *PLOS ONE* 10: e0133591.

3. Pepper J, Hariz M, Zrinzo L (2015): Deep brain stimulation versus anterior capsulotomy for obsessive-compulsive disorder: a review of the literature. *Journal of Neurosurgery* 122: 1028–1037.

4. Stone JL (2001): Dr. Gottlieb Burckhardt the Pioneer of Psychosurgery. *Journal of the History of the Neurosciences* 10: 79–92.

5. Spiegel EA (1954): ANSOTOMY IN PARALYSIS AGITANS. *Arch NeurPsych* 71: 598.

6. Al-Fatly B, Ewert S, Kübler D, Kroneberg D, Horn A, Kühn AA (2019): Connectivity profile of thalamic deep brain stimulation to effectively treat essential tremor. *Brain* 142: 3086–3098.

7. Baldermann JC, Melzer C, Zapf A, Kohl S, Timmermann L, Tittgemeyer M, *et al.* (2019): Connectivity Profile Predictive of Effective Deep Brain Stimulation in Obsessive-Compulsive Disorder. *Biological Psychiatry* 85: 735–743.

8. Coenen VA, Schlaepfer TE, Bewernick B, Kilian H, Kaller CP, Urbach H, *et al.* (2019): Frontal white matter architecture predicts efficacy of deep brain stimulation in major depression [no. 1]. *Translational Psychiatry* 9: 1–10.

9. Horn A, Reich M, Vorwerk J, Li N, Wenzel G, Fang Q, *et al.* (2017): Connectivity Predicts deep brain stimulation outcome in Parkinson disease. *Annals of Neurology* 82: 67–78.

10. Horn A, Wenzel G, Irmen F, Huebl J, Li N, Neumann WJ, *et al.* (2019): Deep brain stimulation induced normalization of the human functional connectome in Parkinson's disease. *Brain* 142: 3129–3143.

11. Irmen F, Horn A, Mosley P, Perry A, Petry-Schmelzer JN, Dafsari HS, *et al.* (2020): Left Prefrontal Connectivity Links Subthalamic Stimulation with Depressive Symptoms. *Annals of Neurology* 87: 962–975.

12. Li N, Baldermann JC, Kibleur A, Treu S, Akram H, Elias GJB, *et al.* (2020): A unified connectomic target for deep brain stimulation in obsessive-compulsive disorder [no. 1]. *Nature Communications* 11: 3364.

13. Mosley PE, Paliwal S, Robinson K, Coyne T, Silburn P, Tittgemeyer M, *et al.* (2019): The structural connectivity of discrete networks underlies impulsivity and gambling in Parkinson's disease. *Brain* 142: 3917–3935.

14. Mosley PE, Paliwal S, Robinson K, Coyne T, Silburn P, Tittgemeyer M, *et al.* (2020): The structural connectivity of subthalamic deep brain stimulation correlates with impulsivity in Parkinson's disease. *Brain* 143: 2235–2254.

15. Petry-Schmelzer JN, Jergas H, Thies T, Steffen JK, Reker P, Dafsari HS, *et al.* (2020): Network Fingerprint of Stimulation-Induced Speech Impairment in Essential Tremor. *Annals of Neurology* n/a. https://doi.org/10.1002/ana.25958

16. Riva-Posse P, Choi KS, Holtzheimer PE, Crowell AL, Garlow SJ, Rajendra JK, *et al.* (2018): A connectomic approach for subcallosal cingulate deep brain stimulation surgery: prospective targeting in treatment-resistant depression [no. 4]. *Molecular Psychiatry* 23: 843–849.

17. Riva-Posse P, Choi KS, Holtzheimer PE, McIntyre CC, Gross RE, Chaturvedi A, *et al.* (2014): Defining Critical White Matter Pathways Mediating Successful Subcallosal Cingulate

Deep Brain Stimulation for Treatment-Resistant Depression. *Biological Psychiatry* 76: 963–969.

18. Sweet JA, Thyagaraj S, Chen Z, Tatsuoka C, Staudt MD, Calabrese JR, *et al.* (2020): Connectivity-based identification of a potential neurosurgical target for mood disorders. *Journal of Psychiatric Research* 125: 113–120.
19. Alhourani A, McDowell MM, Randazzo MJ, Wozny TA, Kondylis ED, Lipski WJ, *et al.* (2015): Network effects of deep brain stimulation. *Journal of Neurophysiology* 114: 2105–2117.
20. Pauls DL, Abramovitch A, Rauch SL, Geller DA (2014): Obsessive-compulsive disorder: An integrative genetic and neurobiological perspective. *Nature Reviews Neuroscience* 15: 410–424.
21. Robbins TW, Vaghi MM, Banca P (2019): Obsessive-Compulsive Disorder: Puzzles and Prospects. *Neuron* 102: 27–47.
22. Abe Y, Sakai Y, Nishida S, Nakamae T, Yamada K, Fukui K, Narumoto J (2015): Hyper-influence of the orbitofrontal cortex over the ventral striatum in obsessive-compulsive disorder. *European Neuropsychopharmacology* 25: 1898–1905.
23. Ahmari SE, Spellman T, Douglass NL, Kheirbek MA, Simpson HB, Deisseroth K, *et al.* (2013): Repeated Cortico-Striatal Stimulation Generates Persistent OCD-Like Behavior. *Science* 340: 1234–1239.
24. Graybiel AM, Rauch SL (2000): Toward a Neurobiology of Obsessive-Compulsive Disorder. *Neuron* 28: 343–347.
25. Harrison BJ, Soriano-Mas C, Pujol J, Ortiz H, López-Solà M, Hernández-Ribas R, *et al.* (2009): Altered Corticostriatal Functional Connectivity in Obsessive-compulsive Disorder. *Arch Gen Psychiatry* 66: 1189.

26. Menzies L, Chamberlain SR, Laird AR, Thelen SM, Sahakian BJ, Bullmore ET (2008): Integrating evidence from neuroimaging and neuropsychological studies of obsessive-compulsive disorder: The orbitofronto-striatal model revisited. *Neuroscience & Biobehavioral Reviews* 32: 525–549.

27. Rotge J-Y, Guehl D, Dilharreguy B, Cuny E, Tignol J, Bioulac B, *et al.* (2008): Provocation of obsessive–compulsive symptoms: a quantitative voxel-based meta-analysis of functional neuroimaging studies. *J Psychiatry Neurosci* 33: 405–412.

28. Saxena S, Brody AL, Schwartz JM, Baxter LR (1998): Neuroimaging and frontal-subcortical circuitry in obsessive-compulsive disorder. *The British Journal of Psychiatry* 173: 26–37.

29. Saxena S, Rauch SL (2000): Functional neuroimaging and the neuroanatomy of obsessive-compulsive disorder. *Psychiatric Clinics of North America* 23: 563–586.

30. Smith EE, Schüller T, Huys D, Baldermann JC, Andrade P, Allen JJB, *et al.* (2020): A brief demonstration of frontostriatal connectivity in OCD patients with intracranial electrodes. *NeuroImage* 117138.

31. McGovern RA, Sheth SA (2017): Role of the dorsal anterior cingulate cortex in obsessive-compulsive disorder: converging evidence from cognitive neuroscience and psychiatric neurosurgery. *Journal of Neurosurgery* 126: 132–147.

32. Milad MR, Rauch SL (2012): Obsessive-compulsive disorder: beyond segregated cortico-striatal pathways. *Trends in Cognitive Sciences* 16: 43–51.

33. Borders C, Hsu F, Sweidan AJ, Matei ES, Bota RG (2018): Deep brain stimulation for obsessive compulsive disorder: A review of results by anatomical target. *Mental Illness* 10: 40–44.

34. Chabardès S, Polosan M, Krack P, Bastin J, Krainik A, David O, *et al.* (2013): Deep Brain Stimulation for Obsessive-Compulsive Disorder: Subthalamic Nucleus Target. *World Neurosurgery* 80: S31.e1-S31.e8.

35. Mallet L, Mesnage V, Houeto JL, Pelissolo A, Yelnik J, Behar C, *et al.* (2002): Compulsions, Parkinson's disease, and stimulation. *Lancet* 360: 1302–1304.

36. Mallet L, Polosan M, Jaafari N, Baup N, Welter M-L, Fontaine D, *et al.* (2008): Subthalamic Nucleus Stimulation in Severe Obsessive–Compulsive Disorder. *New England Journal of Medicine* 359: 2121–2134.

37. Figee M, Luigjes J, Smolders R, Valencia-Alfonso C-E, van Wingen G, de Kwaasteniet B, *et al.* (2013): Deep brain stimulation restores frontostriatal network activity in obsessive-compulsive disorder. *Nature Neuroscience* 16: 386–387.

38. Goodman WK, Foote KD, Greenberg BD, Ricciuti N, Bauer R, Ward H, *et al.* (2010): Deep Brain Stimulation for Intractable Obsessive Compulsive Disorder: Pilot Study Using a Blinded, Staggered-Onset Design. *Biological Psychiatry* 67: 535–542.

39. Nuttin B, Cosyns P, Demeulemeester H, Gybels J, Meyerson B (1999): Electrical stimulation in anterior limbs of internal capsules in patients with obsessive-compulsive disorder. *The Lancet* 354: 1526.

40. Raymaekers S, Vansteelandt K, Luyten L, Bervoets C, Demyttenaere K, Gabriëls L, Nuttin B (2017): Long-term electrical stimulation of bed nucleus of stria terminalis for obsessive-compulsive disorder [no. 6]. *Molecular Psychiatry* 22: 931–934.

41. Jiménez F, Nicolini H, Lozano AM, Piedimonte F, Salín R, Velasco F (2013): Electrical stimulation of the inferior thalamic peduncle in the treatment of major depression and obsessive compulsive disorders. *World Neurosurgery* 80: S30.e17-S30.e25.

42. Lee DJ, Dallapiazza RF, De Vloo P, Elias GJB, Fomenko A, Boutet A, *et al.* (2019): Inferior thalamic peduncle deep brain stimulation for treatment-refractory obsessive-compulsive disorder: A phase 1 pilot trial. *Brain Stimulation* 12: 344–352.

43. Coenen VA, Schlaepfer TE, Goll P, Reinacher PC, Voderholzer U, Elst LT van, *et al.* (2017): The medial forebrain bundle as a target for deep brain stimulation for obsessive-compulsive disorder. *CNS Spectrums* 22: 282–289.

44. Lozano AM, Lipsman N (2013): Probing and Regulating Dysfunctional Circuits Using Deep Brain Stimulation. *Neuron* 77: 406–424.

45. Goodman WK, Price LH, Rasmussen SA, Mazure C, Fleischmann RL, Hill CL, *et al.* (1989): The Yale-Brown Obsessive Compulsive Scale: I. Development, Use, and Reliability. *Arch Gen Psychiatry* 46: 1006–1011.

46. Horn A, Kühn AA (2015): Lead-DBS: A toolbox for deep brain stimulation electrode localizations and visualizations. *NeuroImage* 107: 127–135.

47. Horn A, Li N, Dembek TA, Kappel A, Boulay C, Ewert S, *et al.* (2019): Lead-DBS v2: Towards a comprehensive pipeline for deep brain stimulation imaging. *NeuroImage* 184: 293–316.

48. Yeo BTT, Krienen FM, Sepulcre J, Sabuncu MR, Lashkari D, Hollinshead M, *et al.* (2011): The organization of the human cerebral cortex estimated by intrinsic functional connectivity. *Journal of Neurophysiology* 106: 1125–1165.

49. Holmes AJ, Hollinshead MO, O'Keefe TM, Petrov VI, Fariello GR, Wald LL, *et al.* (2015): Brain Genomics Superstruct Project initial data release with structural, functional, and behavioral measures [no. 1]. *Scientific Data* 2: 150031.

50. Yarkoni T, Poldrack RA, Nichols TE, Van Essen DC, Wager TD (2011): Large-scale automated synthesis of human functional neuroimaging data [no. 8]. *Nature Methods* 8: 665–670.

51. Haynes WIA, Haber SN (2013): The Organization of Prefrontal-Subthalamic Inputs in Primates Provides an Anatomical Substrate for Both Functional Specificity and Integration: Implications for Basal Ganglia Models and Deep Brain Stimulation. *J Neurosci* 33: 4804–4814.

52. Nougaret S, Meffre J, Duclos Y, Breysse E, Pelloux Y (2013): First evidence of a hyperdirect prefrontal pathway in the primate: precise organization for new insights on subthalamic nucleus functions. *Front Comput Neurosci* 7. https://doi.org/10.3389/fncom.2013.00135

53. Petersen MV, Mlakar J, Haber SN, Parent M, Smith Y, Strick PL, *et al.* (2019): Holographic Reconstruction of Axonal Pathways in the Human Brain. *Neuron* 104: 1056-1064.e3.

54. Smith AH, Choi KS, Waters AC, Aloysi A, Mayberg HS, Kopell BH, Figee M (2020): Replicable effects of deep brain stimulation for obsessive-compulsive disorder. *Brain Stimulation*. https://doi.org/10.1016/j.brs.2020.10.016

55. Vlis TAMB van der, Ackermans L, Mulders AEP, Vrij CA, Schruers K, Temel Y, *et al.* (2020): Ventral Capsule/Ventral Striatum Stimulation in Obsessive-Compulsive Disorder: Toward a Unified Connectomic Target for Deep Brain Stimulation? *Neuromodulation: Technology at the Neural Interface* n/a. https://doi.org/10.1111/ner.13339

56. Adler CM, McDonough-Ryan P, Sax KW, Holland SK, Arndt S, Strakowski SM (2000): fMRI of neuronal activation with symptom provocation in unmedicated patients with obsessive compulsive disorder. *Journal of Psychiatric Research* 34: 317–324.

57. Bourne SK, Eckhardt CA, Sheth SA, Eskandar EN (2012): Mechanisms of deep brain stimulation for obsessive compulsive disorder: effects upon cells and circuits. *Front Integr Neurosci* 6. https://doi.org/10.3389/fnint.2012.00029

58. Cheng Y, Xu J, Nie B, Luo C, Yang T, Li H, *et al.* (2013): Abnormal Resting-State Activities and Functional Connectivities of the Anterior and the Posterior Cortexes in

Medication-Naïve Patients with Obsessive-Compulsive Disorder ((L. Fontenelle, editor)). *PLoS ONE* 8: e67478.

59. Fitzgerald KD, Welsh RC, Gehring WJ, Abelson JL, Himle JA, Liberzon I, Taylor SF (2005): Error-related hyperactivity of the anterior cingulate cortex in obsessive-compulsive disorder. *Biological Psychiatry* 57: 287–294.

60. Gruner P, Vo A, Argyelan M, Ikuta T, Degnan AJ, John M, *et al.* (2014): Independent component analysis of resting state activity in pediatric obsessive-compulsive disorder: ICA of Resting State fMRI in Pediatric OCD. *Hum Brain Mapp* 35: 5306–5315.

61. Maia TV, Cooney RE, Peterson BS (2008): The neural bases of obsessive–compulsive disorder in children and adults. *Dev Psychopathol* 20: 1251–1283.

62. Maltby N, Tolin DF, Worhunsky P, O'Keefe TM, Kiehl KA (2005): Dysfunctional action monitoring hyperactivates frontal–striatal circuits in obsessive–compulsive disorder: an event-related fMRI study. *NeuroImage* 24: 495–503.

63. Thorsen AL, Hagland P, Radua J, Mataix-Cols D, Kvale G, Hansen B, van den Heuvel OA (2018): Emotional Processing in Obsessive-Compulsive Disorder: A Systematic Review and Meta-analysis of 25 Functional Neuroimaging Studies. *Biological Psychiatry: Cognitive Neuroscience and Neuroimaging* 3: 563–571.

64. Schlösser RGM, Wagner G, Schachtzabel C, Peikert G, Koch K, Reichenbach JR, Sauer H (2010): Fronto-cingulate effective connectivity in obsessive compulsive disorder: A study with fMRI and dynamic causal modeling. *Hum Brain Mapp* 31: 1834–1850.

65. Whitty CWM, Duffield JE, Tov' PM, Cairns H (1952): Anterior cingulectomy in the treatment of mental disease. *Lancet* 1: 475–481.

66. Jung HH, Chang WS, Rachmilevitch I, Tlusty T, Zadicario E, Chang JW (2015): Different magnetic resonance imaging patterns after transcranial magnetic resonance–guided

focused ultrasound of the ventral intermediate nucleus of the thalamus and anterior limb of the internal capsule in patients with essential tremor or obsessive-compulsive disorder. *JNS* 122: 162–168.

67. Dougherty DD, Baer L, Cosgrove GR, Cassem EH, Price BH, Nierenberg AA, *et al.* (2002): Prospective Long-Term Follow-Up of 44 Patients Who Received Cingulotomy for Treatment-Refractory Obsessive-Compulsive Disorder. *AJP* 159: 269–275.

68. Zuo C, Ma Y, Sun B, Peng S, Zhang H, Eidelberg D, Guan Y (2013): Metabolic Imaging of Bilateral Anterior Capsulotomy in Refractory Obsessive Compulsive Disorder: an FDG PET Study. *J Cereb Blood Flow Metab* 33: 880–887.

69. Tyagi H, Apergis-Schoute AM, Akram H, Foltynie T, Limousin P, Drummond LM, *et al.* (2019): A Randomized Trial Directly Comparing Ventral Capsule and Anteromedial Subthalamic Nucleus Stimulation in Obsessive-Compulsive Disorder: Clinical and Imaging Evidence for Dissociable Effects. *Biological Psychiatry*. https://doi.org/10.1016/j.biopsych.2019.01.017

70. Le Jeune F, Vérin M, N'Diaye K, Drapier D, Leray E, Du Montcel ST, *et al.* (2010): Decrease of Prefrontal Metabolism After Subthalamic Stimulation in Obsessive-Compulsive Disorder: A Positron Emission Tomography Study. *Biological Psychiatry* 68: 1016–1022.

71. Van Laere K, Nuttin B, Gabriels L, Dupont P, Rasmussen S, Greenberg BD, Cosyns P (2006): Metabolic imaging of anterior capsular stimulation in refractory obsessive-compulsive disorder: A key role for the subgenual anterior cingulate and ventral striatum. *Journal of Nuclear Medicine* 47: 740–747.

72. Carmi L, Alyagon U, Barnea-Ygael N, Zohar J, Dar R, Zangen A (2018): Clinical and electrophysiological outcomes of deep TMS over the medial prefrontal and anterior cingulate cortices in OCD patients. *Brain Stimulation* 11: 158–165.

73. Carmi L, Tendler A, Bystritsky A, Hollander E, Blumberger DM, Daskalakis J, *et al.* (2019): Efficacy and Safety of Deep Transcranial Magnetic Stimulation for Obsessive-Compulsive Disorder: A Prospective Multicenter Randomized Double-Blind Placebo-Controlled Trial. *AJP* 176: 931–938.

74. Zhu Y, Fan Q, Zhang H, Qiu J, Tan L, Xiao Z, *et al.* (2016): Altered intrinsic insular activity predicts symptom severity in unmedicated obsessive-compulsive disorder patients: a resting state functional magnetic resonance imaging study. *BMC Psychiatry* 16: 104.

75. Harrison BJ, Pujol J, Cardoner N, Deus J, Alonso P, López-Solà M, *et al.* (2013): Brain Corticostriatal Systems and the Major Clinical Symptom Dimensions of Obsessive-Compulsive Disorder. *Biological Psychiatry* 73: 321–328.

76. Jung WH, Kang D-H, Kim E, Shin KS, Jang JH, Kwon JS (2013): Abnormal corticostriatal-limbic functional connectivity in obsessive–compulsive disorder during reward processing and resting-state. *NeuroImage: Clinical* 3: 27–38.

77. Remijnse PL, Nielen MMA, van Balkom AJLM, Cath DC, van Oppen P, Uylings HBM, Veltman DJ (2006): Reduced Orbitofrontal-Striatal Activity on a Reversal Learning Task in Obsessive-Compulsive Disorder. *Arch Gen Psychiatry* 63: 1225.

78. Shapira NA, Liu Y, He AG, Bradley MM, Lessig MC, James GA, *et al.* (2003): Brain activation by disgust-inducing pictures in obsessive-compulsive disorder. *Biological Psychiatry* 54: 751–756.

79. Stern ER, Welsh RC, Fitzgerald KD, Gehring WJ, Lister JJ, Himle JA, *et al.* (2011): Hyperactive Error Responses and Altered Connectivity in Ventromedial and Frontoinsular Cortices in Obsessive-Compulsive Disorder. *Biological Psychiatry* 69: 583–591.

80. Fridgeirsson EA, Figee M, Luigjes J, van den Munckhof P, Schuurman PR, van Wingen G, Denys D (2020): Deep brain stimulation modulates directional limbic connectivity in obsessive-compulsive disorder. *Brain* 143: 1603–1612.

81. Kuhn J, Baldermann JC (2020): Elucidating neural network changes induced by deep brain stimulation for OCD. *Brain* 143: 1293–1296.

82. Guzick A, Hunt PJ, Bijanki KR, Schneider SC, Sheth SA, Goodman WK, Storch EA (2020): Improving long term patient outcomes from deep brain stimulation for treatment-refractory obsessive-compulsive disorder. *Expert Review of Neurotherapeutics* 20: 95–107.

83. Huys D, Kohl S, Baldermann JC, Timmermann L, Sturm V, Visser-Vandewalle V, Kuhn J (2019): Open-label trial of anterior limb of internal capsule–nucleus accumbens deep brain stimulation for obsessive-compulsive disorder: insights gained. *J Neurol Neurosurg Psychiatry* jnnp-2018-318996.

84. Barcia JA, Avecillas-Chasín JM, Nombela C, Arza R, García-Albea J, Pineda-Pardo JA, *et al.* (2018): Personalized striatal targets for deep brain stimulation in obsessive-compulsive disorder. *Brain Stimulation*. https://doi.org/10.1016/j.brs.2018.12.226

85. Horn A, Fox MD (2020): Opportunities of Connectomic Neuromodulation. *NeuroImage* 117180.

86. Denys D, Mantione M, Figee M, van den Munckhof P, Koerselman F, Westenberg H, *et al.* (2010): Deep Brain Stimulation of the Nucleus Accumbens for Treatment-Refractory Obsessive-Compulsive Disorder. *Arch Gen Psychiatry* 67: 1061.

87. Fox MD, Buckner RL, Liu H, Chakravarty MM, Lozano AM, Pascual-Leone A (2014): Resting-state networks link invasive and noninvasive brain stimulation across diverse psychiatric and neurological diseases. *PNAS* 111: E4367–E4375.

88. Goodman WK, Storch EA, Sheth SA (2021): Harmonizing the Neurobiology and Treatment of Obsessive-Compulsive Disorder. *AJP* 178: 17–29.

89. Shephard E, Stern ER, van den Heuvel OA, Costa DLC, Batistuzzo MC, Godoy PBG, *et al.* (2021): Toward a neurocircuit-based taxonomy to guide treatment of obsessive–compulsive disorder. *Molecular Psychiatry* 1–22.

90. Ewert S, Horn A, Finkel F, Li N, Kühn AA, Herrington TM (2019): Optimization and comparative evaluation of nonlinear deformation algorithms for atlas-based segmentation of DBS target nuclei. *NeuroImage* 184: 586–598.

91. Vogel D, Shah A, Coste J, Lemaire J-J, Wårdell K, Hemm S (2020): Anatomical brain structures normalization for deep brain stimulation in movement disorders. *NeuroImage: Clinical* 27: 102271.

92. Horn A, Neumann W-J, Degen K, Schneider G-H, Kühn AA (2017): Toward an electrophysiological "sweet spot" for deep brain stimulation in the subthalamic nucleus. *Human Brain Mapping* 38: 3377–3390.

93. Kehnemouyi YM, Wilkins KB, Anidi CM, Anderson RW, Afzal MF, Bronte-Stewart HM (2020): Modulation of beta bursts in subthalamic sensorimotor circuits predicts improvement in bradykinesia. *Brain*. https://doi.org/10.1093/brain/awaa394

94. Neumann W-J, Horn A, Ewert S, Huebl J, Brücke C, Slentz C, *et al.* (2017): A localized pallidal physiomarker in cervical dystonia. *Annals of Neurology* 82: 912–924.

95. Nowacki A, Nguyen TA-K, Tinkhauser G, Petermann K, Debove I, Wiest R, Pollo C (2018): Accuracy of different three-dimensional subcortical human brain atlases for DBS – lead localisation. *NeuroImage: Clinical* 20: 868–874.

96. Rappel P, Grosberg S, Arkadir D, Linetsky E, Snineh MA, Bick AS, *et al.* (2020): Theta-alpha Oscillations Characterize Emotional Subregion in the Human Ventral Subthalamic Nucleus. *Movement Disorders* 35: 337–343.

97. Tinkhauser G, Shah SA, Fischer P, Peterman K, Debove I, Nygyuen K, *et al.* (2019): Electrophysiological differences between upper and lower limb movements in the human subthalamic nucleus. *Clinical Neurophysiology* 130: 727–738.

98. van Wijk BCM, Pogosyan A, Hariz MI, Akram H, Foltynie T, Limousin P, *et al.* (2017): Localization of beta and high-frequency oscillations within the subthalamic nucleus region. *NeuroImage: Clinical* 16: 175–183.

99. Husch A, V. Petersen M, Gemmar P, Goncalves J, Hertel F (2017): PaCER - A fully automated method for electrode trajectory and contact reconstruction in deep brain stimulation. *Neuroimage Clin* 17: 80–89.

100. Duffley G, Anderson DN, Vorwerk J, Dorval AD, Butson CR (2019): Evaluation of methodologies for computing the deep brain stimulation volume of tissue activated. *J Neural Eng* 16: 066024.

101. Gunalan K, Chaturvedi A, Howell B, Duchin Y, Lempka SF, Patriat R, *et al.* (2017): Creating and parameterizing patient-specific deep brain stimulation pathway-activation models using the hyperdirect pathway as an example. *PLOS ONE* 12: e0176132.

102. Åström M, Diczfalusy E, Martens H, Wårdell K (2015): Relationship between Neural Activation and Electric Field Distribution during Deep Brain Stimulation. *IEEE Transactions on Biomedical Engineering* 62: 664–672.

103. Butenko K, Bahls C, Schröder M, Köhling R, Rienen U van (2020): OSS-DBS: Open-source simulation platform for deep brain stimulation with a comprehensive automated modeling. *PLOS Computational Biology* 16: e1008023.

104. Noecker AM, Frankemolle-Gilbert AM, Howell B, Petersen MV, Beylergil SB, Shaikh AG, McIntyre CC (2021): StimVision v2: Examples and Applications in Subthalamic Deep

Brain Stimulation for Parkinson's Disease. *Neuromodulation: Technology at the Neural Interface* n/a. https://doi.org/10.1111/ner.13350

105. Wang Q, Akram H, Muthuraman M, Gonzalez-Escamilla G, Sheth SA, Oxenford S, *et al.* (2021): Normative vs. patient-specific brain connectivity in deep brain stimulation. *NeuroImage* 224: 117307.

106. Greene DJ, Marek S, Gordon EM, Siegel JS, Gratton C, Laumann TO, *et al.* (2020): Integrative and Network-Specific Connectivity of the Basal Ganglia and Thalamus Defined in Individuals. *Neuron* 105: 742-758.e6.

107. Jakab A, Werner B, Piccirelli M, Kovács K, Martin E, Thornton JS, *et al.* (2016): Feasibility of Diffusion Tractography for the Reconstruction of Intra-Thalamic and Cerebello-Thalamic Targets for Functional Neurosurgery: A Multi-Vendor Pilot Study in Four Subjects. *Front Neuroanat* 10. https://doi.org/10.3389/fnana.2016.00076

108. Cui Z, Li H, Xia CH, Larsen B, Adebimpe A, Baum GL, *et al.* (2020): Individual Variation in Functional Topography of Association Networks in Youth. *Neuron* 106: 340-353.e8.

109. de Almeida Marcelino AL, Horn A, Krause P, Kühn AA, Neumann W-J (2019): Subthalamic neuromodulation improves short-term motor learning in Parkinson's disease. *Brain* 142: 2198–2206.

110. Lofredi R, Auernig GC, Irmen F, Nieweler J, Neumann W-J, Horn A, *et al.* (2020): Subthalamic stimulation impairs stopping of ongoing movements. *Brain*. https://doi.org/10.1093/brain/awaa341

111. Neumann W-J, Schroll H, Marcelino de A, Luisa A, Horn A, Ewert S, *et al.* (2018): Functional segregation of basal ganglia pathways in Parkinson's disease. *Brain* 141: 2655–2669.

112. Johnson KA, Duffley G, Foltynie T, Hariz M, Zrinzo L, Joyce EM, *et al.* (2020): Basal Ganglia Pathways Associated with Therapeutic Pallidal Deep Brain Stimulation for

Tourette Syndrome. *Biological Psychiatry: Cognitive Neuroscience and Neuroimaging*. https://doi.org/10.1016/j.bpsc.2020.11.005

113. Lewin AB, De Nadai AS, Park J, Goodman WK, Murphy TK, Storch EA (2011): Refining clinical judgment of treatment outcome in obsessive–compulsive disorder. *Psychiatry Research* 185: 394–401.

114. Pauli WM, Nili AN, Tyszka JM (2018): A high-resolution probabilistic *in vivo* atlas of human subcortical brain nuclei. *Scientific Data* 5: 180063.

115. Ewert S, Plettig P, Li N, Chakravarty MM, Collins DL, Herrington TM, *et al.* (2018): Toward defining deep brain stimulation targets in MNI space: A subcortical atlas based on multimodal MRI, histology and structural connectivity. *NeuroImage* 170: 271–282.

116. Amunts K, Lepage C, Borgeat L, Mohlberg H, Dickscheid T, Rousseau M-É, *et al.* (2013): BigBrain: An Ultrahigh-Resolution 3D Human Brain Model. *Science* 340: 1472–1475.

117. Polosan M, Droux F, Kibleur A, Chabardes S, Bougerol T, David O, *et al.* (2019): Affective modulation of the associative-limbic subthalamic nucleus: deep brain stimulation in obsessive–compulsive disorder. *Translational Psychiatry* 9: 73.

Supplemental Information

Patient cohort

Data of 50 obsessive-compulsive disorder (OCD) patients from four centers were included into our analyses, comprising 22 anterior limb of the internal capsule (ALIC) deep brain stimulation (DBS) patients from University Hospital of Cologne, 14 subthalamic nucleus (STN) DBS patients from Grenoble University Hospital, eight patients from Hospital Clínico San Carlos in Madrid with bilateral electrodes targeting the nucleus accumbens (NAcc), and six patients from the National Hospital for Neurology and Neurosurgery in London with electrodes implanted to both STN and ALIC. Patients operated in Cologne, Grenoble and Madrid centers had received two DBS leads each (N = 44 patients with N = 88 leads), while the six patients from the London cohort were implanted with four DBS leads each (N = 6 patients with N = 24 leads). All patients gave written informed consent, and study protocols received ethical clearance from each local Ethics Committee.

Imaging

For all patients, high-resolution structural T1-weighted images were acquired on a 3.0-Tesla MRI scanner before surgery. Postoperatively, computed tomography (CT) was obtained in 33 patients to evaluate lead placement, while eleven patients from the Grenoble cohort and the six London patients received postoperative MRI. Across the four centers, pre- and postoperative OCD symptom severity was assessed on the Yale-Brown Obsessive-Compulsive Scale (Y-BOCS) (1). In the London cohort, multiple stimulation settings with combined “optimized” settings of both targets (and respective Y-BOCS improvement scores) vs. the ones where each target was probed alone (STN

vs. ALIC zones) were available (2). When calculating maps for patients stimulated in each target alone, the latter scores and stimulation settings were used. Instead, when calculating overall models across all patients, the “optimized” settings were used.

Electrode localizations and estimation of stimulation effects

DBS electrodes were localized using default parameters in Lead-DBS software (http://www.lead-dbs.org) and details are reported elsewhere (3,4). Briefly, postoperative CT and MRI scans were linearly coregistered to preoperative T1 images using Advanced Normalization Tools (ANTs, http://stnava.github.io/ANTs/; (5)). This registration was further corrected for brain shift as implemented in Lead-DBS.

Electrodes were then pre-localized using either the PaCER algorithm (6) for postoperative CT, or the TRAC/CORE algorithm (7) for postoperative MRI, and automatic pre-localizations were manually refined by an expert user (NL). Volumes of tissue activated (VTAs) were estimated based on patients’ individual stimulation parameters using a finite element method (FEM) (4). A volume conductor model was constructed via a four-compartment mesh that includes grey and white matter, lead contacts, and insulating parts. The electric field (E-field) distribution was simulated using an adaptation of the FieldTrip-SimBio pipeline integrated into Lead-DBS (https://www.mrt.uni-jena.de/simbio/; http://fieldtriptoolbox.org/), and thresholded at 0.2 V/mm to obtain binarized VTAs (4).

Based on preoperative acquisitions, volumes were then normalized into ICBM 2009b Nonlinear Asymmetric (“MNI”) template space using the SyN approach implemented in ANTs, with an additional subcortical refinement step (“Effective: Low Variance + Subcortical Refinement” preset in Lead-DBS). This specific method was top performer for subcortical image registrations in a recent comparative study that involved >10,000 nonlinear warps and a variety of normalization techniques (8), as

confirmed by a second comparative study from a different group (9). Coregistration and normalization results were reviewed and refined if needed. Subsequently, DBS electrodes were reconstructed via Lead-DBS software and warped into MNI space.

DBS connectivity modeling

This section is dedicated to a more detailed description of our approach to modeling functional connectivity R-maps. Specifically, functional connectivity analyses were based on a normative functional connectome, calculated from resting-state functional MRI (rs-fMRI) scans of 1,000 healthy subjects (10) that had been acquired within the Brain Genomics Superstruct Project (https://dataverse.harvard.edu/dataverse/GSP; (11)).

For each of the 50 OCD patients, normative whole-brain functional connectivity seeding from bilateral VTAs was estimated similarly as done in previous work (12,13): First, voxel-wise correlations between mean time-series of voxels inside each bilateral VTA and time-series of all remaining whole-brain voxels were calculated. This analysis was repeated 1,000 times per patient, using data of each of the 1,000 healthy subjects in the normative connectome. Second, the resulting 1,000 connectivity *fingerprints* for each patient were averaged and Fisher-z-transformed. Given individual differences in electrode position, stimulation parameter settings, and consequently, divergent VTA seeds, this approach resulted in 50 average connectivity fingerprints (i.e., one for each OCD patient).

On a voxel-by-voxel basis, individual fingerprints were then correlated with Y-BOCS improvements across patients to generate an *R-map model* of “optimal” connectivity profiles for maximal Y-BOCS improvement. This R-map models regions to which DBS electrodes optimally should or should not be connected to maximize Y-BOCS improvement. Rs-fMRI derived functional connectivity being bipolar (i.e.,

anticorrelations across time series existing (14)), blue regions can also mean that the BOLD signal obtained from the electrode seeds should be negatively correlated with the one recorded in these regions for optimal Y-BOCS improvement.

Inverted map calculation

As described in the methods section, the inverted map highlights brain regions which have cortical connectivity profiles most similar to the optimal ones defined by the agreement map. Specifically, similarity between each brain voxel's connectivity profile (based on a precomputed resting-state functional MRI connectome) and the (cortical) agreement map was calculated. Since the goal here was to define the optimal (subcortical) neuromodulation sites, we chose to restrict the agreement map to cortical regions when calculating the inverted map based on it in order to avoid circularity. Had subcortical regions been included in the agreement map, the generated inverted map could have been biased, since the subcortical voxels will have maximum connectivity (R=1) to themselves. However, again, this step did not alter results. To demonstrate this, in **Figure S1**, we show that the result stays largely unchanged when we do not exclude the subcortical regions before calculating the inverted map. These two versions of the inverted maps (based on the full agreement map and cortical only agreement maps) were highly similar (spatial correlation $R=0.96$, $p<1e-17$).

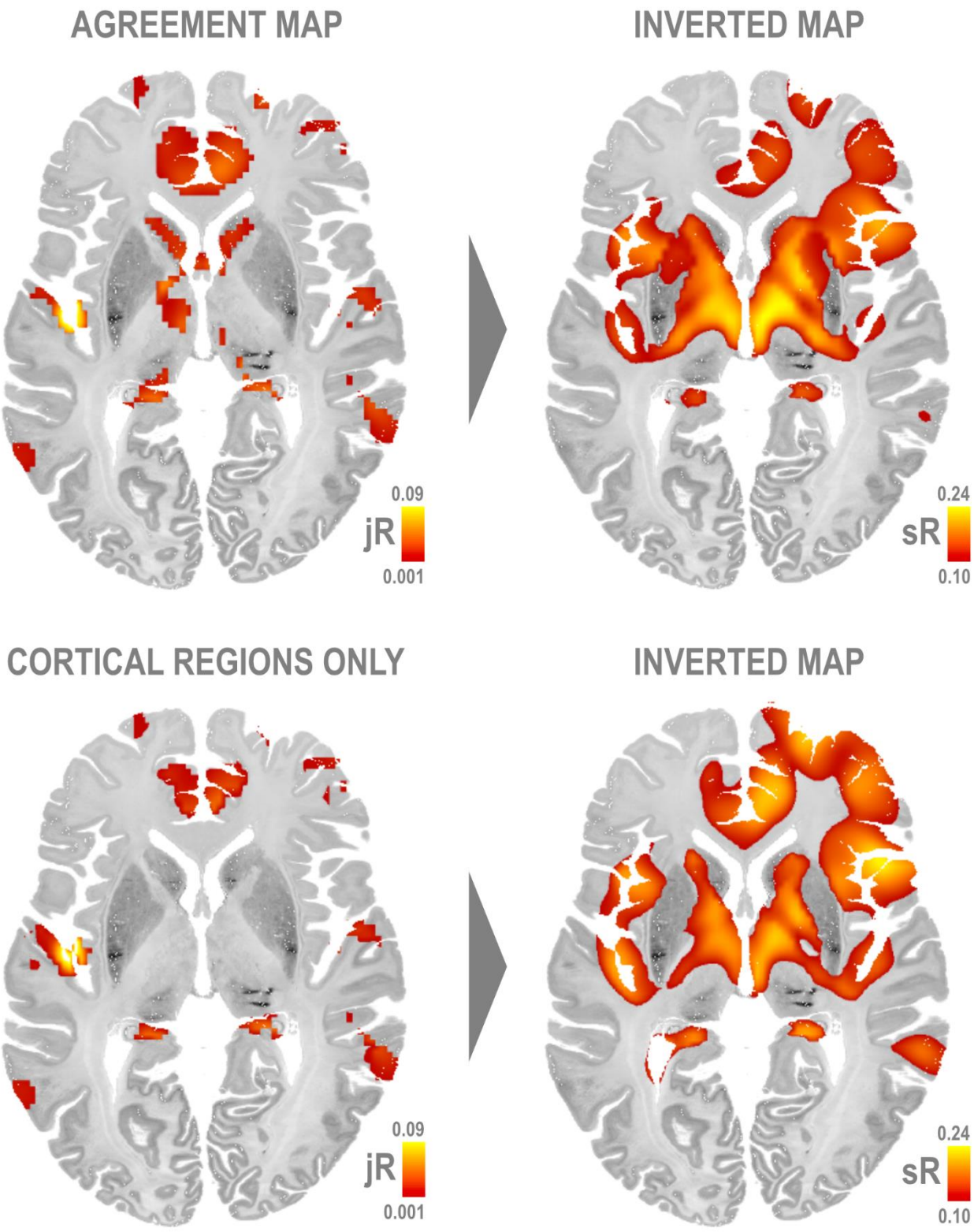

Figure S1. *Inverted maps based on the full agreement map and its cortical regions only. Top left panel shows the full agreement map calculated based on the R-maps from the ALIC and STN cohorts. Bottom left shows the same map restricted to cortical (and cerebellar) regions. Inverted maps shown in the right panels were calculated by testing each brain voxel's connectivity profile (based on a precomputed resting state functional MRI connectome) with its similarity to either version of the agreement map. The analysis shows that restricting the agreement map to cortical regions did not alter results. ALIC, anterior limb of the internal capsule; STN, subthalamic nucleus.*

Prominent anatomical regions of maps

In order to extract spatial information about the anatomical structures highlighted by the different statistical maps, we parcellated each target-specific R-map, agreement map and inverted map according to a Talairach atlas version transformed into MNI space (15). We selected this atlas because of its detailed description and the availability of Brodmann areas labeling. The atlas is freely available to download from the FMRIB Software Library (FSL). The peak value in addition to voxel coordinates (x/y/z in MNI space) were next extracted for each parcel using an in-house MATLAB code implemented in Lead-DBS. We reported highest 30-40% of parcels in each of the resulting statistical maps. For ALIC and STN targets, results were manually analyzed using 3Dslicer software (www.slicer.org).

Table S1: Anatomical regions associated with optimal clinical improvement across the four different models. Regions identified with optimal connectivity profiles across the brain are listed, as well (Inverted Map column)

Reg.	Hem.	ALIC R-map	STN R-map	Full Cohort R-map	Agreement Map	Inverted Map
			Positive Peak Coordinates X/Y/Z (R-Value)			
ACC (BA 24, 32)	RH	5/4/39.5 (0.54)	18/12/48 (0.26)	6/6/39.5 (0.60)	9/41/0 (0.05)	8/32/22 (0.27)
	LH	-8/5/37 (0.53)	-16/40/18 (0.08)	-6.5/10/31 (0.53)	-3/37/10 (0.03)	-1/36/16 (0.24)
ALIC	RH		13/9.5/-2.5 (0.48)	16/4/5.5 (0.31)		12/9/-2 (0.20)
	LH		-13.5/7.5/-2.5 (0.49)	-16.5/7.5/2 (0.26)		-11/6/-3 (0.24)
CBM	RH	5/-56/-17 (0.45)	18/-50/-28 (0.16)	4/-71.5/-14.5 (0.58)	14/-44/-34 (0.09)	18/-48/-36 (0.10)
	LH	-2.5/-56/-16 (0.46)	-14/-58/-32 (0.17)	-4.5/-60/-16 (0.51)	-44/-46/-46 (0.06)	-16/-64/-20 (0.06)
Cun. (BA 17)	RH	18/-82/10 (0.18)	8.5/-102/9 (0.30)	14/-83/10 (0.49)		
	LH	-14/78/14 (0.21)	-8/-104/3 (0.48)	-11/-77.5/11 (0.42)		
dlPFC (BA 46, 9, 9/46)	RH	32.5/44.5/29 (0.35)		40/54.5/27 (0.42)		26/44/34 (0.26)
	LH	-34/42/34 (0.34)		-40/50/27 (0.45)		-26/38/30 (0.18)
IFG (BA 10, 46)	RH		24/24.5/-17 (0.31)			42/12/-18 (0.19)
	LH		-26/31/-14.5 (0.21)			-38/12/-16 (0.30)
Ins. (BA 13)	RH	44/4/-2 (0.6)	48/-2/-8 (0.32)	39.5/-25/6.5 (0.59)	47/-3.5/-3.5 (0.07)	36/14/-10 (0.34)
	LH	-40.5/-18.5/2 (0.53)	-44/4/-10 (0.35)	-46.5/-4/6 (0.61)	-47/-9.5/-1 (0.10)	-38/12/-10 (0.33)
IPL (BA 7, 39)	RH	65.5/-27/30.5 (0.5)		61/-35/47 (0.50)		60/-42/30 (0.26)
	LH	-67/-29/26 (0.5)		-52.2/-41/29 (0.58)		-64/-40/32 (0.15)
MCC (BA 23, 31)	RH	8.5/-15/34 (0.53)	8/-41/39.5 (0.29)	6/-22/41.5 (0.48)	12/-44/44 (0.13)	18/-56/32 (0.26)
	LH	-8/-29/39.5 (0.53)	-1.5/-33.5/40 (0.20)	-11/-35.5/40 (0.61)	-12/-42/42 (0.17)	-10/-72/34 (0.23)
MD	RH	8/-20/2 (0.41)	6/-10/10 (0.08)	6/-20/2 (0.55)		4/-18/4 (0.2)
	LH	-6/-20/2 (0.38)	-6/-16/2 (0.09)	-6/-20/2 (0.54)		-4/-10/0 (0.2)
Prec. (BA 7, 31)	RH	14/-66/39.5 (0.46)	8/-50/44 (0.34)	14/-64/42 (0.58)	14/-66/32 (0.13)	18/-56/32 (0.26)
	LH	-14/-63/38.5 (0.50)	-1/-57/47.5 (0.35)	-12/-44/44 (0.60)	-16/-68/30 (0.09)	-10/-72/34 (0.23)
SFG (BA 9, 11)	RH		22/50/-26 (0.35)			22/42/32 (0.26)
	LH		-8/56/-34 (0.31)			-26/38/30 (0.18)
SMA (BA 6)	RH	5/-3/66.5 (0.47)		3.5/-1.5/66 (0.56)		
	LH	-9.5/-1.5/70 (0.43)		-6.5/-4/70 (0.54)		
STN	RH	9/-14/-7 (0.46)	10/-12/-8 (0.31)	9.5/-14.5/-7 (0.51)	10/-10/-8 (0.16)	9/-10/-6 (0.24)

	LH	-9.5/-17.5/-8 (0.43)	-6/-12/-6 (0.34)	-7/-16/-7 (0.50)	-6/-12/-8 (0.15)	-9/-10/-7 (0.24)
Uncus (BA 28)	RH	22/-10/-36 (0.52)	16/0/-28 (0.32)	20/-2/-40 (0.51)	22/-05/-36 (0.08)	22/0/-36 (0.32)
	LH	-17/-4/-38.5 (0.43)	-14/2/-26 (0.25)	-14/0/-40 (0.55)	-21/-6/-35 (0.07)	-20/-4/-36 (0.25)
		Negative Peak Coordinates X/Y/Z (R-Value)				
CBM	RH	21.5/-87/-39 (-0.53)	13/-49/-17 (-0.34)	32/-90/-40 (-0.62)	32/-83/-43 (-0.07)	16/-78/-44 (-0.24)
	LH	-30/-92/-22 (-0.45)	-1/-49/-17 (-0.35)	-22/-90/-38 (-0.62)	-34/87/-43 (-0.02)	-20/-90/-38 (-0.08)
IFG (BA 10, 46)	RH	49/25/4.5 (-0.25)	48/26/4 (-0.21)	47/27/-19 (-0.37)	62/24/20 (-0.01)	64/12/32 (-0.10)
	LH	-48/18.5/10 (-0.45)	-54/48/-6 (-0.28)	-39.5/23/-18 (-0.44)	-58/20/20 (-0.04)	-60/18/30 (-0.16)
IPL (BA 7, 39)	RH	35/-33.5/56 (-0.36)		53/-63/41.5 (-0.38)		
	LH	-43/-35/56 (-0.37)		-44/-67/45 (-0.42)		
MTG (BA 19, 39)	RH	46/-7/30 (-0.59)	38/-64/22 (-0.16)	66/0/-20.5 (-0.58)	56/-44/-16 (-0.01)	56/-44/-16 (-0.10)
	LH	-64/-14.5/-17 (-0.50)	-36/-58/18 (-0.40)	-65.5/-9/-14 (-0.57)	-56/-43/-14.5 (-0.04)	-52/-42/-16 (-0.20)
OL (BA 18, 19)	RH			26/-95/-4.5 (-0.52)	35.5/-85/-5 (-0.04)	
	LH			-29/-96/-1 (-0.52)	-39/-80/-3.5 (-0.04)	
PCL (BA 3, 4)	RH	5/26.5/63 (-0.49)	2/-25.5/71 (-0.15)	3.5/-36/66.5 (-0.60)	6.5/-24/67.5 (-0.14)	12/-22/72 (-0.18)
	LH	-4.5/-35.5/64 (-0.46)	-1/-31/73.5 (-0.22)	-3/-30/63 (-0.59)	-3.5/-30/67.5 (-0.11)	-10/-26/72 (-0.19)
Prec. (BA 7, 31)	RH	4/-61.5/41 (-0.50)		1/-56/34 (-0.48)		
	LH	-5/-57.5/39.5 (-0.45)		-1/-62.5/34 (-0.44)		
SFG (BA 9, 11)	RH	7.5/65/22 (-0.41)	2/15.5/64 (-0.40)	11/65.5/13.5 (-0.52)	14/34/42 (-0.01)	-10/60/34 (-0.11)
	LH	-12/66/22 (-0.53)	-4/7/64.5 (-0.44)	-14.5/66/20 (-0.57)	-8/52/44 (-0.05)	-10/52/44 (-0.12)

Abbreviations: **ACC**, anterior cingulate cortex; **ALIC**, anterior limb of the internal capsule; **BA**, Brodmann area; **CBM**, cerebellum; **Cun.**, cuneus; **dlPFC**, dorsolateral prefrontal cortex; **Hem.**, hemisphere; **IFG**, inferior frontal gyrus; **Ins.**, insula; **IPL**, inferior parietal lobule; **LH**, left hemisphere; **MCC**, midcingulate cortex; **MD**, medial dorsal nucleus of thalamus; **MTG**, middle temporal gyrus; **OL**, occipital lobule; **PCL**, paracentral lobule; **Prec.**, precuneus; **Reg.**, region; **RH**, right hemisphere; **SFG**, superior frontal gyrus; **SMA**, supplementary motor area; **STN**, subthalamic nucleus.

Supplemental References

1. Goodman WK, Price LH, Rasmussen SA, Mazure C, Fleischmann RL, Hill CL, *et al.* (1989): The Yale-Brown Obsessive Compulsive Scale: I. Development, Use, and Reliability. *Arch Gen Psychiatry* 46: 1006–1011.
2. Tyagi H, Apergis-Schoute AM, Akram H, Foltynie T, Limousin P, Drummond LM, *et al.* (2019): A Randomized Trial Directly Comparing Ventral Capsule and Anteromedial Subthalamic Nucleus Stimulation in Obsessive-Compulsive Disorder: Clinical and Imaging Evidence for Dissociable Effects. *Biol Psychiatry*. https://doi.org/10.1016/j.biopsych.2019.01.017
3. Li N, Baldermann JC, Kibleur A, Treu S, Akram H, Elias GJB, *et al.* (2020): A unified connectomic target for deep brain stimulation in obsessive-compulsive disorder [no. 1]. *Nat Commun* 11: 3364.
4. Horn A, Li N, Dembek TA, Kappel A, Boulay C, Ewert S, *et al.* (2019): Lead-DBS v2: Towards a comprehensive pipeline for deep brain stimulation imaging. *NeuroImage* 184: 293–316.
5. Avants BB, Tustison N, Song G (2009): Advanced normalization tools (ANTS). *Insight J* 2: 1–35.
6. Husch A, V. Petersen M, Gemmar P, Goncalves J, Hertel F (2017): PaCER - A fully automated method for electrode trajectory and contact reconstruction in deep brain stimulation. *NeuroImage Clin* 17: 80–89.
7. Horn A, Kühn AA (2015): Lead-DBS: A toolbox for deep brain stimulation electrode localizations and visualizations. *NeuroImage* 107: 127–135.
8. Ewert S, Horn A, Finkel F, Li N, Kühn AA, Herrington TM (2019): Optimization and comparative evaluation of nonlinear deformation algorithms for atlas-based segmentation of DBS target nuclei. *NeuroImage* 184: 586–598.

9. Vogel D, Shah A, Coste J, Lemaire J-J, Wårdell K, Hemm S (2020): Anatomical brain structures normalization for deep brain stimulation in movement disorders. *NeuroImage Clin* 27: 102271.

10. Yeo BTT, Krienen FM, Sepulcre J, Sabuncu MR, Lashkari D, Hollinshead M, *et al.* (2011): The organization of the human cerebral cortex estimated by intrinsic functional connectivity. *J Neurophysiol* 106: 1125–1165.

11. Holmes AJ, Hollinshead MO, O'Keefe TM, Petrov VI, Fariello GR, Wald LL, *et al.* (2015): Brain Genomics Superstruct Project initial data release with structural, functional, and behavioral measures [no. 1]. *Sci Data* 2: 150031.

12. Al-Fatly B, Ewert S, Kübler D, Kroneberg D, Horn A, Kühn AA (2019): Connectivity profile of thalamic deep brain stimulation to effectively treat essential tremor. *Brain* 142: 3086–3098.

13. Horn A, Reich M, Vorwerk J, Li N, Wenzel G, Fang Q, *et al.* (2017): Connectivity Predicts deep brain stimulation outcome in Parkinson disease. *Ann Neurol* 82: 67–78.

14. Li M, Dahmani L, Wang D, Ren J, Stocklein S, Lin Y, *et al.* (2021): Co-activation patterns across multiple tasks reveal robust anti-correlated functional networks. *NeuroImage* 227: 117680.

15. Lancaster JL, Tordesillas-Gutiérrez D, Martinez M, Salinas F, Evans A, Zilles K, *et al.* (2007): Bias between MNI and Talairach coordinates analyzed using the ICBM-152 brain template. *Hum Brain Mapp* 28: 1194–1205.